Surface Science Reports 72 (2017) 369–391

Contents lists available at ScienceDirect

Surface Science Reports

journal homepage: www.elsevier.com/locate/surfrep

Electrokinetic mechanism of wettability alternation at oil-water-rock interface

Huanhuan Tian, Moran Wang*

Department of Engineering Mechanics and CNMM, Tsinghua University, Beijing, 100084, China

ARTICLE INFO

Article history:
Received 3 November 2017
Received in revised form
28 December 2017
Accepted 29 December 2017
Available online 9 January 2018

Keywords:
Wettability alteration
Electrical double layer interaction
Ion exchange
Electrokinetics
Liquid-solid interface

ABSTRACT

Design of ions for injection water may change the wettability of oil-brine-rock (OBR) system, which has very important applications in enhanced oil recovery. Though ion-tuned wettability has been verified by various experiments, the mechanism is still not clear. In this review paper, we first present a comprehensive summarization of possible wettability alteration mechanisms, including fines migration or dissolution, multicomponent ion-exchange (MIE), electrical double layer (EDL) interaction between rock and oil, and repulsive hydration force. To clarify the key mechanism, we introduce a complete frame of theories to calculate attribution of EDL repulsion to wettability alteration by assuming constant binding forces (no MIE) and rigid smooth surface (no fines migration or dissolution). The frame consists of three parts: the classical Gouy-Chapman model coupled with interface charging mechanisms to describe EDL in oil-brine-rock systems, three methods with different boundary assumptions to evaluate EDL interaction energy, and the modified Young-Dupré equation to link EDL interaction energy with contact angle. The quantitative analysis for two typical oil-brine-rock systems provides two physical maps that show how the EDL interaction influences contact angle at different ionic composition. The result indicates that the contribution of EDL interaction to ion-tuned wettability for the studied system is not quite significant. The classical and advanced experimental work using microfabrication is reviewed briefly on the contribution of EDL repulsion to wettability alteration and compared with the theoretical results. It is indicated that the roughness of real rock surface may enhance EDL interaction. Finally we discuss some pending questions, perspectives and promising applications based on the mechanism.

1. Introduction

Ion-tuned wettability, which means the dependence of wettability on variation of brine ionic composition in an oil-brine-rock (OBR) system, has attracted increasing interests due to its important applications in oil industry. Electrokinetic interactions play a critical role in the mechanism debate on ion-tuned wettability. In the following, the background, experimental evidence and mechanism debate of ion-tuned wettability will be introduced in sequence, and finally the objectives and structure of this review will be presented.

1.1. Background: ion-designed waterflooding

Waterflooding has been pervasively applied in oil recovery for about one century [1]. Recently, it has drawn extensive attention on that the ionic composition of injected brine can influence waterflooding efficiency in both sandstone and carbonate reservoirs.

About twenty years ago, Morrow and his coworkers reported improved waterflooding efficiency in sandstones by decreasing the salinity of the injected water [2–4], which is now referred to as low salinity waterflooding (LSF). The benefit brought by LSF is usually called low salinity effect (LSE). Three working conditions for LSE were justified by Tang and Morrow [4]: (1) significant clay fraction, (2) presence of connate water, and (3) exposure to crude oil to form mixed-wet rock surface. Since then, amounts of laboratory tests [5–14], well tests [15–21] and modeling work [22–26] have been launched to verify, explain and predict LSE. Generally speaking, LSF can increase oil recovery by 5%–20% original oil in place (OOIP) [27] in sandstones. Counter examples of LSE were rare, one of which was given by Ref. [5] and was possibly due to the presence of chlorite. Besides salinity, researchers also reported the effect of cation valence on flooding efficiency in sandstones [3,28,29], which was relied on the specific OBR system.

* Corresponding author.
E-mail address: mrwang@tsinghua.edu.cn (M. Wang).

https://doi.org/10.1016/j.surfrep.2018.01.001
0167-5729/

Carbonates are usually more oil-wet and fractured compared with sandstones, causing traditional waterflooding hard to benefit [30]. One exceptional success is the injection of seawater into the Ekofisk chalk field in the North Sea since 1988 [30], which has motivated researchers to clarify the effects of brine ionic composition on flooding efficiency in carbonates. Austad and his co-workers [30–33] have proved that relatively plentiful SO_4^{2-} in seawater can improve spontaneous imbibition especially at high temperature, which is simultaneously influenced by Ca^{2+} and Mg^{2+}. Seawater flooding (SWF) can improve oil recovery by 40%–60% OOIP [27]. Researchers have been exploring more ways to modify the injected brine for optimized oil recovery in carbonates [34–43], such as modifying seawater or formation water by directly diluting, deleting NaCl, or adding potential determining ions, as well as designing totally artificial brine. Generally speaking, brine with high content of certain potential determining ions and low total salinity may bring the most benefits.

In this review, these new waterflooding strategies by manipulating brine ionic composition are referred to as ion-designed flooding (IDF). IDF is environment-friendly and economical, compared with regular enhanced oil recovery methods such as thermal recovery and chemical flooding, and thus is considered promising.

It is commonly believed that the increased oil recovery by IDF is due to the alteration of reservoir to more water-wet conditions [27,44,45], which is denoted as ion-tuned wettability in this review. Actually this issue has been studied early even before the prosperity of IDF [46–54], but it is only recently that the benefits behind it have been emphasized.

1.2. Experimental evidence of ion-tuned wettability

The wettability of an OBR system can be measured in two scales. Pore-scale wettability is usually measured by contact angle and surface forces for smooth surfaces, while Darcy-scale wettability is usually measured by displacing behaviors of a rock sample. We will introduce the experimental evidence of ion-tuned wettability in these two scales in the following.

1.2.1. Pore-scale wettability

Contact angle measurements for OBR systems can be difficult. Due to the chemical and geometrical heterogeneity, contact angle hysteresis of OBR systems may be very significant [1,55–57], with the equilibrium contact angle ranging between receding contact angle θ_R and advancing contact angle θ_A. Sessile drop method or captive drop method can be used to provide one equilibrium contact angle value for each drop, and repeated measurements may be needed to present the alteration trends with ionic composition. θ_R and θ_A can also be measured directly by numerous methods, such as adhesion test [1,52], tilting plate method [55], modified sessile drop method with two plates [55], dynamic Wilhelmy plate method [58] and so on. One thing to declare is that the contact angle is usually measured in water-phase for OBR systems, thus a lower contact angle means a more water-wet system.

The surface forces between oil-functionalized tip and rock surface measured by atomic force microscopy (AFM) can also indicate the wettability of OBR systems. The smaller adhesion or stronger repulsion means more water-wet conditions. Besides, water film thickness is another indication of wettability. Thicker water films mean more water-wet OBR systems.

(1) For sandstones

In recent twenty years, various measurements of contact angle or surface forces have been reported for sandstones. Up to our knowledge, most experiments reported contact angle increase with the decrease of pH (in the pH range 3–9) [51–54,59] and the increase of cation valence [3,59]. However, the trend with salinity can be non-monotonic and highly related with the components of the OBR system.

If cations in the brine are all monovalent, the OBR system may first become more oil-wet and then more water-wet with the concentration decreasing from 1 M to 10^{-5} M. The early standard adhesion tests of crude oil-NaCl (aq)-glass/mica systems have indicated that higher concentration lead to more water-wet conditions in the range 0.01 M–1 M [51–53]. This is also consistent with the captive contact angle and surface forces between asphalene-functionalized AFM tip and mica measured by Ref. [54]. In addition, the latter paper presented the "wettability map" for a larger range of concentration, showing the concentration lower than 0.01 M can make the system to more water-wet. It also declared that the turning point should be dependent on the OBR system. It should be mentioned that the trend of contact angle variation may be drowned by the measurement error. For example, Morrow et al. [3] attached decane drops onto crude oil-aged quartz surface immersed in single-component chloride brine, and used dynamic Wilhelmy plate method to measure contact angle. With the measurement error as high as ±10° and the large hysteresis, they observed no consistent trend of contact angle variation with concentration.

Consistent with LSE, if the original brine contains both mono- and multi-valence cations, brine with salinity down below 5000 ppm can make the OBR system more water-wet in pore-scale [59–62]. For example, Nasralla et al. [60] used captive drop method to measure contact angle of crude oil-brine-mica system at different conditions (500–1000 psi, 140-250 °F), and reported contact angle decrease of 3–13° by diluting aquifer water (TDS = 5436 ppm) for ten times, and 15–39° by changing formation water (TDS = 174156 ppm) to deionized water. Another example is given by Mahani et al. [61], who carefully attached layers of clay particles onto glass slide to imitate the real sandstone surface, and measured contact angle of sessile crude oil drops. They reported contact angle decrease of more than 90° by diluting brine for 4–16 times (original TDS = 25950 ppm). Furthermore, Hilner et al. [62] measured the adhesion between alkane-functionalized AFM tip and sand grains, with brine salinity in the range of 1500–28500 ppm. The results showed that adhesion was constant for high salinity and decreased significantly for salinity below 5000–8000 ppm. However, higher than 5000 ppm, lower salinity does not necessary lead to more water-wet conditions in pore-scale for multicomponent brine. According to [60], seawater (TDS = 54680 ppm) showed higher contact angle compared with formation water (TDS = 174156 ppm), though the former has a lower salinity and less multivalent cations.

(2) For carbonates

There are still limited pore-scale wettability measurements for carbonates. In 2010, Yousef et al. [34] measured contact angle of captive crude oil drop below low-permeability carbonate plates in reservoir conditions, and reported similar contact angle for seawater and field connate water, contact angle decrease from 90° to 63° when seawater was 20 times diluted, and almost no further decrease when seawater was 100 times diluted. In 2012, Yi and Sarma [39] monitored the contact angle of crude oil drops on core plates, and reported enhanced water-wetness by lowering salinity or adding SO_4^{2-} at 90 °C. In 2014, Mahani et al. [42] used sessile drop method to measure contact angle, and found seawater and diluted

seawater altered carbonates to more water-wet compared with formation water.

1.2.2. Darcy-scale wettability

Darcy-scale wettability can be presented by displacement behaviors [1,55]. For example, imbibition test measures the volume of oil displaced from oil-saturated sample by spontaneous imbibition of brine with time. Qualitatively, higher imbibition rate and volume indicate more water-wet conditions. Quantitative measurement of wettability based on displacement behaviors can be given by Amott test or USBM method [1,55].

During the development of IDF, imbibition tests are commonly launched together with flooding tests. From these imbibition tests, it can be concluded that smaller cation valence [3,29] and lower salinity [3–5] make sandstones more water-wet, and the more potential determining ions [30–33] and lower salinity [36,39] make carbonates more water-wet. There are another several works indicating the ion-tuned wettability for carbonates. Webb et al. [63] measured imbibition capillary pressure of North Sea carbonate under reservoir condition. In 2010, Fathi et al. [43] used chromatographic wettability test to measure the dependence of wettability on brine. They reported that seawater and seawater depleted in NaCl both made the OBR system more water-wet compared with the original formation water, but directly diluting seawater did not cause such wettability alteration.

Generally speaking, low salinity and small cation valence make sandstones more water-wet in Darcy scale. Both multi- and single-component brine can cause the wettability alteration. For carbonates, the adding of potential determining ions and the depleting of NaCl can make the system more water-wet in Darcy scale.

1.3. Mechanism debate on ion-tuned wettability

In spite of increasing interests, the mechanism of ion-tuned wettability is still not clear, especially for low salinity effect. Various mechanisms have been proposed by emphasizing different ion-related interfacial interactions. The most famous three to explain wettability alteration during LSF in sandstones are (*i*) fines migration due to enhanced EDL repulsion between clay particles [4], (*ii*) enhanced electrical double layer (EDL) repulsion between oil and clay [64], (*iii*) multicomponent ion exchange (MIE) which breaks ion binding and ligand binding between oil and rock [7], and which causes pH increase and thus reduces interface tension [65,66]. No consensus has been reached on the dominant mechanism. For SWF in carbonates, the conditions are much clearer. MIE which releases the adsorbed oil molecules on carbonate surface should dominate carbonate wettability alteration by seawater, and Austad and his coworkers have identified the roles of several potential determining ions (SO_4^{2-}, Ca^{2+} and Mg^{2+}) in this process [30–33,43]. However, similar to the conditions for sandstones, it is still under debate whether fines migration or dissolution [40], enhanced EDL repulsion between oil and rock [42], or enhanced MIE [33,35] dominates wettability alteration by low salinity.

Besides the above frequently-emphasized mechanisms to make the OBR system water-wet at low salinity, two mechanisms that may have opposite effects must be paid attention to, either. Firstly, when oil and rock are oppositely charged, the attractive EDL interaction can be produced [67]. Secondly, the half-hydrated ions adsorbed onto the charged interface can make water molecules crowded, leading to a repulsive hydration force [54,56]. These two mechanisms can enhance the water-wetness of the OBR system with high salinity brine.

Actually all the mechanisms mentioned before are all related with electrokinetics. Of course EDL interaction between oil and rock is directly related with electrokinetics. Fines migration or dissolution emphasizes the destruction and re-building of flow structure. MIE and hydration force are highly related with surface charges which may be influenced by the EDLs between oil and rock. Thus we believe these two are indirectly related with electrokinetics. In this review, we are referring to EDL interaction (which can be attractive or repulsive) between oil and rock when we mention the electrokinetic mechanism of ion-tuned wettability.

In this review, we mainly focus on the electrokinetic mechanism of ion-tuned wettability, for the following reasons. Firstly, the existence of EDL interaction between oil and rock is universal and definite. In comparison, fines migration or dissolution is not always observed, MIE may not be important when the original brine contains no multivalent ions, and the dependence of hydration force on salinity is only strong for high salinity and some specific interfaces, as discussed in Sec. 2. Therefore, the clarification of the concrete contribution of EDL interaction to ion-tuned wettability must be important. Secondly, though the theory of EDL interaction has been developed for about a century in colloid science, and the extension to wettability alteration has also been developed, it has not been commonly used to quantitatively predict contact angle variation. Therefore, it is important to evaluate the existing theories, so we can expand its applicability in some extent, and conclude the intrinsic defects of it and present the perspectives.

1.4. Objectives and structure of this review

There are three objectives of this review. Firstly, we aim to present an overview of the role of EDL interaction in ion-tuned wettability, including its competitions with other important OBR interactions. Secondly, we aim to integrate the existing theories of the contribution of EDL interaction to ion-tuned wettability, carefully evaluate the assumptions and give some suggestions. Lastly, we aim to improve the understanding of ion-tuned wettability by quantitatively analyzing two typical OBR systems and qualitatively compare the results with experiments.

This review is organized as below. Firstly, we will review the OBR interactions in Sec. 2, focusing on a comprehensive summarization of the possible mechanisms of ion-tuned wettability, including fines migration or dissolution, MIE, EDL interaction, and hydration force. In Sec. 3–5, we will present a theoretical framework of the contribution of EDL interaction to ion-tuned wettability, including the description of the EDL in OBR systems, the calculation of EDL interaction energy, and the dependence of contact angle on EDL interaction. In these three sections, we take two specific OBR systems, in one of which oil and rock are similarly charged while in the other oil and rock are oppositely charged, as examples to analyze. In Sec. 6, we will discuss some open questions and the possible perspectives. Finally, the conclusion will be given in Sec. 7.

2. Overview of oil-brine-rock interactions

In this section, we will firstly introduce the concepts of oil-brine-rock interactions, and then review the four possible mechanisms of ion-tuned wettability which emphasize different interactions.

2.1. Concepts

OBR interactions determine the wettability of OBR systems. Generally speaking, OBR interactions can be categorized by whether they cause attraction (or binding, adsorption) or repulsion between oil and rock.

The attractive interactions involve acid/base interaction, ion

binding, ligand bridging, van der Waals force, and surface precipitation [7,48,49,68]. They make the OBR system more oil-wet. Most of them involve interface charge, which will be described before introducing the five attractive interactions. Contacting with brine, acid groups of rock and oil can lose protons while base groups can obtain protons, which can make rock and oil negatively or positively charged. Actually even for totally nonpolar oil, some other mechanisms, such as hydroxyl adsorption, may also cause oil-brine interface charge [69,70]. Usually sandstones and oil are negatively charged and carbonates are positively charged in formation conditions.

Acid/base interaction: The charged polar groups of oil can adsorb onto oppositely charged rock, which is called acid/base interaction. The competition between salt cations and protonated base groups of oil to adsorb on to the negatively charged rock surface is also called cation exchange, while that between salt anions and deprotonated acid groups of oil onto the positively charged rock surface s also called anion exchange. The acid/base interaction can be influenced by the ionic distribution near charged interface, so it is also seen as EDL attraction in this review.

Ion binding: If both oil and rock are similarly charged, multivalent counter-ions can act as bridges between these two interfaces. If multivalent cation bridges negatively charged oil and rock, this mechanism is also referred to as cation bridging, which is common in sandstones. Note that this interaction is essentially electrostatic and no ligand forms.

Ligand binding: If oil and rock simultaneously form ligands with the bridging multivalent ions, the adsorption may be very strong, which interaction is called ligand binding.

Van der Waals forces: This interaction includes both polar and non-polar molecular interactions, and is ubiquitously existed regardless of the interface charges and the components of OBR systems. Van der Waals forces can be attractive or repulsive between two phases in a medium, but usually it is attractive in an OBR system due to the high permittivity of brine [56].

Surface precipitation: If the oil is a poor solvent for asphaltenes, the asphaltenes may precipitate on the rock and alter the surface to more oil-wet.

Other attractive interactions suggested in the literature, such as water bridging, are relatively weak or not common in OBR systems. Acid/base interaction, ion binding and ligand binding are strongly influenced by the ionic composition. If these bindings are weakened or removed, the OBR system will become more water-wet.

Besides the above attractive interactions, repulsive interactions are also critical to determine the wettability of OBR systems. EDL repulsion and steric forces are the most important two repulsive interactions [46], as discussed below.

EDL repulsion: Charged interface in brine can attract counter-ions and repel co-ions, forming the structure of electrical double layer (EDL). Two EDLs developed between two similarly charged surfaces may overlap each other at small distances, resulting in a repulsive force. The details will be shown in Sec. 3.

Hydration force: The counter-ions adsorbed on the charged interfaces are usually half-hydrated, causing a strong repulsion when two surfaces approach each other to the molecular scale. This force is also referred to as steric or solvation force.

The intensity of EDL repulsion is mainly determined by the EDL thickness and the surface charging quantities, which depend on brine ionic composition including potential determining ions (very small content could lead to large zeta potential variation, e.g. H^+, OH^- for silica, oil and SO_4^{2-} for calcite), ion valence and concentration. Ionic composition may also influence hydration force under some conditions, as discussed in Sec. 2.5. Stronger repulsive interactions make the OBR system more water-wet.

In addition to all the above interactions, the clay-clay interaction in sandstones can influence wettability, too. Sandstone surface is usually covered with clays. EDL repulsion between clay particles is an essential part of clay-clay interaction, thus brine composition which enhances EDL repulsion can destruct clay structures. This will further influence the wettability of the OBR system, since inner and exterior clay particles show different hydrophilicity. This will be discussed in detail in Sec. 2.2.

With an overview of OBR interactions, we can have a better understanding of the wettability of OBR systems. For example, now we can easily explain why carbonates are more oil-wet than sandstones. In formation conditions, usually crude oil and sandstones are negatively charged, while carbonates are positively charged. Thus EDL repulsion occurs in sandstone reservoirs and makes them more water-wet, and acid/base interaction (or EDL attraction) occurs in carbonate reservoirs and makes them more oil-wet. In addition, we can summarize that acid/base interaction (or EDL attraction), ion binding, ligand binding, EDL repulsion, hydration force, and clay-clay interaction can all contribute to ion-tuned wettability. Therefore, the mechanism debate on ion-tuned wettability is actually the debate on which of the interactions dominates ion-tuned wettability under different conditions, as introduced in Sec. 2.2–2.6 as shown in Fig. 1.

2.2. Fines migration and dissolution

Fines migration and dissolution emphasize the role of clay-clay interaction in ion-tuned wettability. Limited fines migration was first suggested by Ref. [4] to explain wettability alteration during LSF in sandstones. The authors proposed this theory based on the three working conditions for LSE clarified by their flooding tests (existence of connate water, clay, and crude oil aging) and the observed limited fines in the effluent. The authors pointed out that, under formation conditions with high-salinity connate brine, the originally water-wet clay particles on rock surface may turn to partially oil-wet during the long-time contact to crude oil. They assumed that, during low salinity waterflooding, the connection between clays is reduced due to the enhanced EDL repulsion. Therefore, the mixed-wet clay particles as well as the crude oil adsorbed on it can be released from the rock surface, as shown in Fig. 2(a), and the OBR system becomes more water-wet since the inner water-wet clay particles are exposed to brine. Nevertheless, the mechanism is doubtful because effluent fines are not commonly observed [45]. However, some researchers emphasize the role of fines migration in LSF in sandstones in a different way. They suggested that instead of altering wettability, fines migration may block pore throats and divert flow, and thus increases microscopic sweep efficiency and oil recovery [27,44]. If so, fines just

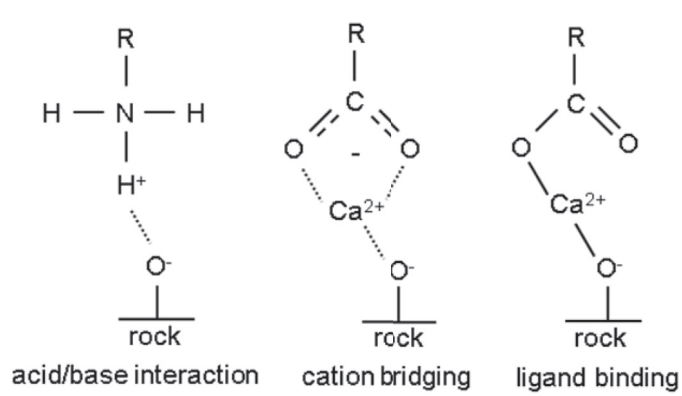

Fig. 1. Schematics for examples of some attractive interactions.

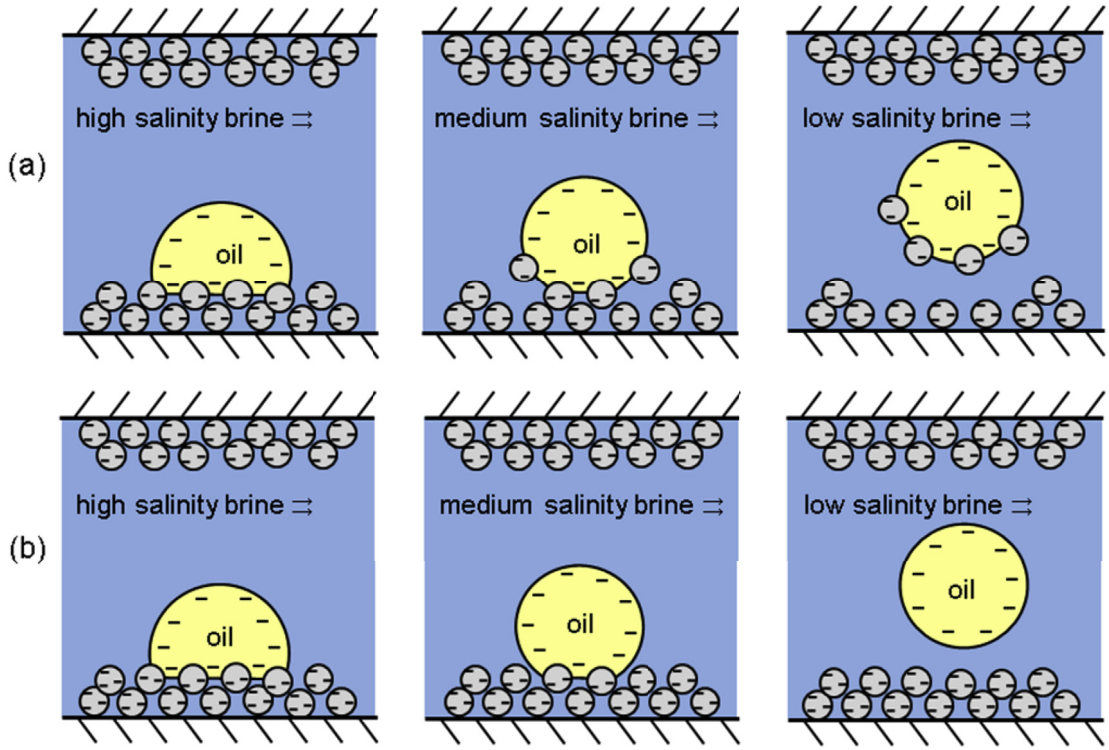

Fig. 2. Schematics of (a) limited fines migration and (b) EDL repulsion between oil and clay. Sandstone rock surface is usually covered with clay particles, as represented by the grey rounds.

change their location in rock matrix and may not release at all, but still play an important role in LSF. This idea still need to be carefully validated, and is not in the scope of ion-tuned wettability.

Similarly, for carbonates, it is also proposed that the improvement of microscopic sweep efficiency can partly explain LSE [40]. Besides, mineral dissolution has also been emphasized in different aspects. For example, Austad et al. [35] suggested that the dissolution of anhydrite ($CaSO_4$) during LSF can release more SO_4^{2-} to the brine, which can enhance MIE and alter the OBR system to more water-wet. This is also discussed in Sec. 2.4. In addition, based on the observation of Ca^{2+} increase in the effluent during LSF and the EMR tests, it was suggested that mineral dissolution occurred and was possibly able to improve the connectivity between micropores and macropores, thus improve oil recovery [34,40]. However, no fines migration or dissolution has been observed by the wettability tests of [42].

To summarize, fines migration or dissolution may contribute to some wettability alteration, but the more important effect of it on IDF may be the change of flow structure. Besides, the existence of fines migration or dissolution has not been proved a universal phenomenon during IDF.

2.3. Multicomponent ion exchange

MIE stresses the role of ion exchange to break or form acid/base interaction, ion binding, and ligand binding in ion-tuned wettability. MIE was first proposed by Lager et al. [7] in 2006 to explain LSE in sandstones. The main idea is, during LSF, because the number of multivalent cations is decreased, ion bindings or ligand bindings between oil and clay can be broken. This causes the release of organic polar compounds and organo-metallic complexes which are connected to the surface by multivalent ions, and makes the OBR system more oil-wet. If this is true, it can be inferred that no LSE can be detected if multivalent ions are removed from the connate water. The authors designed an experiment to prove the mechanism. They brushed the core by high-salinity NaCl solution until no multivalent ions were effluent, then aged the core with crude oil, and finally flooded the core with NaCl solution of different salinities. In this way, no LSE was found, which supported the MIE mechanism. Note that this theory does not deny the acting of other mechanisms of ion-tuned wettability when multivalent ions exist in connate brine. In another paper, the authors claimed that EDL repulsion enhanced by low salinity water may assist the MIE process by offsetting the ion binding interaction [17].

MIE which causes pH change may also contribute to ion-tuned wettability in sandstones. Based on the fact that the effluent water was found alkalescent, McGuire et al. [65] proposed that the increased pH in formation during LSF can cause saponification or emulsification, and thus reduce interfacial tension (IFT) of oil-brine interface and make the OBR system more water-wet, just like alkaline flooding. However, experiment data from abundant literature indicates that the effluent water is not alkaline enough to cause the above effects [7,45]. Later, Austad et al. [66] proposed a local pH increase theory. The theory assumes that the adsorbed Ca^{2+} on clay surface can be replaced by H^+ in low salinity brine, leading to local pH increase. This will further make the adsorbed acids and bases of oil released, thus the OBR system becomes more water-wet. In 2015, Underwood et al. [71] reported a molecular dynamics simulation that gave a pore-scale support for this mechanism. Actually local pH increase is only a phenomenon of a kind of MIE mechanism, thus we regard that it belongs to MIE mechanisms, too.

Nevertheless, it has been proved that MIE cannot be the only mechanism dominating ion-tuned wettability in sandstones. The MIE discussed above emphasizes the releasing of multivalent ions from the clay surface to bulk solution. However, as indicated by both experiments and simulation, a “self-freshening zone” without

multivalent ions forms at the low salinity water front, and increased oil recovery is observed as long as this zone reaches the production well [72]. Obviously in the self-freshening zone the MIE described before cannot take effect, so there must be another mechanism which significantly changes wettability.

MIE is also proposed to explain the wettability alteration by seawater in carbonates, and bears little controversy. After a series of work to identify the role of potential determining ions, Zhang et al. [33] elaborated a comprehensive MIE mechanism. According to their theory, SO_4^{2-} is a strong potential determining ion that can make carbonates negatively charged. Then Ca^{2+} and Mg^{2+} are able to approach carbonate surface and substitute the absorbed carboxylic group or Ca^{2+}-carboxylic complex, and thus make carbonates more water-wet.

However, it is still not clear how and how much MIE contributes to the wettability alteration by low salinity water in carbonates. As supposed by Fathi et al. [43], when NaCl concentration is high in brine, the EDL is highly compacted, and SO_4^{2-}, Ca^{2+} and Mg^{2+} should compete with Na^+ to approach the carbonate surface. Therefore, when NaCl is depleted from brine, SO_4^{2-}, Ca^{2+} and Mg^{2+} can have better access to the carbonate surface, enhancing MIE and making the system more water-wet. This idea needs further validation. Austad et al. [35] proposed that anhydrite in carbonate matrix is necessary for LSE in carbonates, since the dissolution of anhydrite in low salinity water can release SO_4^{2-} and enhance MIE. Nevertheless, in some experiments LSE is observed in cores without anhydrite [40].

To summarize, MIE is used to explain ion-tuned wettability from different points of view. MIE is unlikely to dominate ion-tuned wettability individually, and it may act with other mechanisms to take effect.

2.4. EDL interaction

EDL interaction between charged interfaces can be attractive or repulsive, depending on the interface charges. In this part, we only talk about the EDL interaction between oil and rock, not involving that between clay particles. Though important for fines release from the rock surface, the EDL repulsion between clays cannot explain LSE without clarification of fines migration and flow structure alteration in the rock matrix. In contrast, the EDL interaction between oil and rock can explain ion-tuned wettability independently, as discussed below. Besides, EDL attraction talked here emphasizes different aspects of acid/base interaction as MIE. MIE emphasizes the breaking or forming of acid/base interaction by ion exchange, while here the EDL attraction emphasizes the weakening of acid/base interaction by ionic distribution near the charged interface.

EDL repulsion occurs when oil and rock are similarly charged, and EDL repulsion theory has been introduced to oil industry during the exploration of OBR interactions. In 1989, Buckley et al. [47] used EDL repulsion theory to predict the adhesion of crude oil onto glass for varied pH and concentration of NaCl solution. The theory is partly consistent with experiment data; however, it cannot explain the non-adhesion of oil at high concentration. In 1991, Hirasaki [46] described a complete frame to calculate the influence of surface forces (van der Waals forces, EDL repulsion, and structural forces) on contact angle. This paper does not present the comparison between the theory and experiments.

With the development of IDF, the role of EDL repulsion in ion-tuned wettability has attracted increasing attention. In 2009, Ligthelm et al. [64] proposed that, during LSF in sandstones, enhanced EDL repulsion between clay and oil may overcome the attractive interactions such as cation bridging, making the OBR system more water-wet, as shown in Fig. 2(b). In the last few years several experiments [59–61,73] reported that the alteration trend of contact angle with salinity is correlated with that of zeta potential, and then claimed the contribution of EDL repulsion to the wettability alteration. Especially, Mahani et al. [61] emphasized that clay morphology could enhance the effect of EDL repulsion. Similarly, once carbonates are altered to negatively charged by injected brine, EDL repulsion can be used to explain LSE in carbonates. In 2015, Mahani et al. [42] reported more negative zeta potential and smaller contact angle for diluted seawater compared with formation water and seawater, to support the EDL repulsion mechanism. However, the above experiments cannot deny the role of MIE in ion-tuned wettability; furthermore, zeta potential itself cannot determine the strength of EDL repulsion, as discussed in Sec. 5.

Enhanced EDL attraction can make the OBR system more oil-wet when the oil and the rock are oppositely charged, which may appear in sandstones with plentiful multivalent cations and is common in carbonates without wettability modification by seawater. EDL attraction can be enhanced or weakened by low salinity, depending on the specific charging conditions. There are two examples. Mugele et al. [74] reported positive zeta potential of the mica-$CaCl_2$ solution interface for high concentration and pH, and used EDL interaction theory to predict the dependence of contact angle on ionic composition of the $CaCl_2$ solution-decane-mica system. The theory is well consistent with experiments, presenting the contact angle decrease for low salinity and low pH. Another support of the role of EDL attraction in ion-tuned wettability is given by Ref. [67], which reports that if oil and rock are oppositely charged, higher salinity leads to more water-wet conditions.

2.5. Repulsive hydration force

The repulsive hydration force was firstly observed between solid hydrophilic surfaces by SFA experiments [56]. Hydrophilic solids are usually charged in brine due to ionization of surface groups. Therefore, they can attract counter-ions from the brine, and the counter-ions are especially compacted very near the solid surface, which zone is called Stern layer. In the Stern layer, since ions are usually half-hydrated, the water molecules can also be highly compacted and ordered. This can produce a repulsive hydration force when the distance between two surfaces becomes lower than about 1–2 nm. If the charged surface groups are not extruded into the brine (the van der Waals plane and Helmholtz plane are very close), which is true for mica, the hydration force can be highly dependent on brine ionic composition. To summarize, the repulsion can be observed only for concentration higher than a critical value, and this critical value is larger for more-hydrated ions; plus, the repulsion can be enhanced by high concentration and high hydration numbers of the counter-ions.

The repulsive hydration force has also been claimed as an important OBR interaction. Even before the prosperity of IDF, it has been used to explain the enhanced water-wetness for high concentration in the standard adhesion tests of crude oil-NaCl (aq)-mica/glass system [47,52–54]. However, since it can alter the wettability inversely to the LSE, it is not commonly emphasized during the mechanism debate for ion-tuned wettability.

2.6. Summary and discussion

Based on the previous review in this section, we may clarify the distinction and relation between the four possible mechanisms of ion-tuned wettability. The ion binding, ligand binding, acid/base

interactions can act together to make the system more oil-wet. Then by changing the ionic composition of brine, MIE can break these connections by removing the binding ions or substituting adsorbed oil molecules with simple ions, and EDL attraction can be weakened or EDL repulsion can be enhanced to reduce the binding force. Besides, for some interfaces, repulsive hydration force can be enhanced with high salinity and high cation valence. Fines migration or dissolution mainly changes the inner structure of the rock, and its effect on ion-tuned wettability may be not universal. These mechanisms may act together or compete with each other according their dependence on ionic composition.

In addition, it is clear that EDL interaction is most universal in OBR systems. Oil and rock contacting with brine are always charged, so EDL interaction is produced. Fines migration or dissolution is not always observed by experiments. MIE emphasizes the involvement of multivalent ions on OBR interactions, and may not be important when considering the salinity effect on wettability for 1:1 electrolyte. Plus, the dependence of hydration force on salinity is only strong for high salinity and some specific interfaces. Therefore, it must be important to understand how much EDL interaction can influence wettability, to provide a basis to analyze the effects of other mechanisms under specific conditions.

3. EDL in oil-brine-rock systems

The charged interface and the liquid zone with redistributed ions by Coulombic force are respectively the first and the second layer of the electrical double layer, as introduced in detail in Sec. 3.1. The EDL in oil-brine-rock systems will be fully described in this section. First, the concepts of classical electrical double layer (EDL), and the basic functions for the ionic distribution in the second layer will be given in Sec. 3.1. Then, the relations to determine interface charging quantities will be introduced in Sec. 3.2–3.4, including the electrostatic equilibrium condition, and the charging models of rock-brine and oil-brine interfaces. Next, the boundary conditions for two interacting EDLs, including the constant charge (CC), constant potential (CP), and charge regulation (CR) boundaries, will be discussed in 3.5. Finally, the charging quantities of two typical OBR systems will be analyzed in 3.6. This section establishes the basis for the analysis of EDL interaction energy in Sec. 4.

3.1. Classical EDL theory

Materials immiscible and immersed in electrolyte solution are usually charged due to dissociation of surface groups, specific adsorption of ions, or orientation of water molecules [47,69,75]. We denote the interface potential as ϕ_0 and the total interface charge density as σ_0. The charged interface forms the first layer of EDL. It attracts counter-ions and repels co-ions, making the ion distribution near the interface distinctive from that in the bulk electrolyte. This layer near interface in electrolyte forms the second layer of EDL, and can be further divided as Stern layer and diffuse layer, as introduced below. Very near the interface, counter-ions are strongly attracted and cannot move vertically to the interface, which zone is referred to as the Stern layer. The plane where the outer ions of Stern layer locate is called the outer Helmholtz plane. Out of the outer Helmholtz plane, the ions can diffuse in all directions but are still influenced by interface charge, which zone is called the diffuse layer. The imagining plane separating immobile and mobile ions is called the slip plane, where the electrical potential is named as ζ potential. Usually the outer Helmholtz plane and the slip plane are very close to each other and undistinguishable. In this paper, we denote the sum of the charge densities of the charged interface and the Stern layer as equivalent interface charge

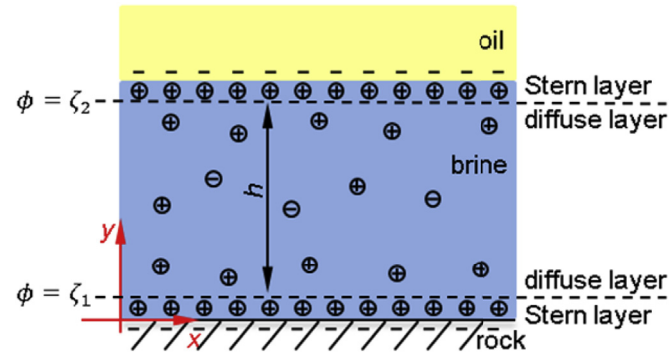

Fig. 3. The scheme for classical EDLs between oil and rock. The charged interface forms the first layer of EDL. Stern layer and diffuse layer combine to form the second layer of EDL.

σ_d, which is balanced by the diffuse layer charge density under the electric neutrality condition. Without differentiating the outer Helmholtz plane and the slip plane, the simple structure of EDL is shown in Fig. 3.

Poisson-Boltzmann (PB) equation is a classical description of diffuse layer. Its derivation, assumptions, and some analytical solutions will be briefly introduced below.

Poisson equation is commonly used to describe the relationship between electrical field and local charge density under the continuity hypothesis:

$$\nabla\cdot(\varepsilon_0\varepsilon_r\nabla\phi) = -\rho_e, \tag{1}$$

where ε_0 is the vacuum permittivity, ε_r the relative permittivity, ϕ the electrical potential, and ρ_e the local net charge density. ρ_e satisfies $\rho_e = \sum_i z_i e N_A c_i$, where z_i and c_i are respectively the valence and concentration of the i-th ion, e the electron charge and N_A the Avogadro number. $N_A c_i$ may also be denoted as n_i in the following. Ions in equilibrium follow Boltzmann distribution in ideal solution:

$$c_i = c_i^\infty \exp(-z_i e\phi/k_b T), \tag{2}$$

where c_i^∞ is the bulk concentration, k_b the Boltzmann constant, and T the temperature. Supposing ε_r does not vary with location, the combination of Eqs. (1) and (2) leads to the famous PB equation:

$$\nabla^2\phi = -\frac{eN_A}{\varepsilon_0\varepsilon_r}\sum_i z_i c_i^\infty \exp(-z_i e\phi/k_b T). \tag{3}$$

The following analysis is based on the system shown in Fig. 3. To non-dimensionalize Eq. (3), two characteristic quantities are defined: ionic strength $I = \sum_i z_i^2 c_i/2$, with the concentration unit; and Debye parameter $\kappa = \sqrt{2e^2 N_A I/\varepsilon_0\varepsilon_r k_b T}$, with the unit reciprocal to length. The EDL thickness is usually estimated as 3–5 κ^{-1}. By substituting $C_i^\infty = c_i^\infty/I$, $\psi = e\phi/k_b T$, and $Y = y\kappa$ into Eq. (3), we get

$$\frac{d^2\psi}{dY^2} = -\frac{1}{2}\sum_i z_i C_i^\infty \exp(-z_i\psi), \tag{4}$$

with boundary conditions $\psi(Y=0) = \psi_{d1} = e\zeta_1/k_b T$ and $\psi(Y = h\kappa) = \psi_{d2} = e\zeta_2/k_b T$, where subscript 1 represents rock-brine interface, and 2 represents oil-brine interface, as shown in Fig. 3. In some cases, Eq. (4) is rewritten as the following form:

$$\frac{d}{dY}\left(\frac{d\psi}{dY}\right)^2 = \frac{d}{dY}\sum_i C_i^\infty \exp(-z_i\psi), \tag{5}$$

whose dimensional form is also commonly used:

$$\frac{d}{dy}\left(\frac{d\phi}{dy}\right)^2 = \frac{2k_bT}{\varepsilon_0\varepsilon_r}\frac{d}{dy}\sum_i n_i. \tag{6}$$

Eq. (5) or Eq. (6) can be integrated twice to get the analytical solution of single EDL ($\psi_{d1} = \psi_d$, $\psi_{d2} = 0$ and $h = \infty$) for 1:1 electrolyte [76]:

$$\psi = 2\ln\frac{1+\tanh(\psi_d/4)\exp(-Y)}{1-\tanh(\psi_d/4)\exp(-Y)}. \tag{7}$$

For 2:1 and 1:2 electrolytes, the analytical solution can also be derived, with more complex forms [77]. In addition, Eq. (5) or Eq. (6) can also combine with the Gauss law to give the electrostatic equilibrium conditions of EDL, as described in Sec. 3.2.

For two interacting EDLs, Eq. (4) has to be numerically solved. However, if $|\psi| < 1$, typically $|\zeta| < 25$ mV at 298 K, Debye-Hückel approximation ($\sinh\psi \approx \psi$) can be applied to Eq. (4) for 1:1 electrolyte, and thus Eq. (4) can be approximately solved as [78].

$$\psi = (\sinh\kappa h)^{-1}(\psi_{d2}\sinh\kappa y + \psi_{d1}\sinh(\kappa h - \kappa y)), \tag{8}$$

which is widely used to estimate EDL interaction energy, as discussed in Sec. 4.

In real OBR systems, ζ_1, ζ_2 are dependent on ionic composition and water film thickness, and can be determined by the coupling of electrostatic equilibrium conditions (introduced in Sec. 3.2) and interface charging models (introduced in Sec. 3.3 and 3.4). This full description of interface charging quantities for two interacting EDLs is referred to as charge regulation, which means that charging quantities can vary with interface distance. For simplicity, constant potential or constant charge condition may be used instead of charge regulation, as discussed in Sec. 3.5.

3.2. Electrostatic equilibrium condition

Electrostatic equilibrium condition is commonly used to help determine interface charging quantities and EDL interaction energy. It describes the relation between the electrical field $\boldsymbol{E}_s$ on the slip plane and the equivalent charging density σ_d,

$$\sigma_d = \varepsilon_0\varepsilon_r\boldsymbol{E}_s\cdot\boldsymbol{n}, \tag{9}$$

where $\boldsymbol{n}$ is the normal direction of the slip plane (pointing to the water phase). Eq. (9) is given by the Gauss Law. $\boldsymbol{E}_s$ has an implicit relation with ζ according to PB equation, thus the electrostatic equilibrium condition actually gives a relation between σ_d and ζ. For the two interfaces shown in Fig. 3,

$$\sigma_{d1} = -\varepsilon_0\varepsilon_r\left.\frac{d\phi}{dy}\right|_{y=0}, \quad \sigma_{d2} = \varepsilon_0\varepsilon_r\left.\frac{d\phi}{dy}\right|_{y=h}. \tag{10}$$

Eq. (10) can be rewritten to avoid differentiation, as introduced below. The combination of Eq. (10) with Eq. (6) leads to

$$\sigma_{d1}^2 - \sigma_{d2}^2 = 2N_A\varepsilon_0\varepsilon_r k_bT\sum_i c_i^\infty(\exp(-z_i\psi_{d1}) - \exp(-z_i\psi_{d2})). \tag{11}$$

For a single EDL, Eq. (11) can be degraded to the famous Grahame equation

$$\sigma_d^2 = 2N_A\varepsilon_0\varepsilon_r k_bT\sum_i c_i^\infty(\exp(-z_i\psi_d) - 1). \tag{12}$$

Besides, the electric neutrality condition for the system shown in Fig. 3 leads to

$$\sigma_{d1} + \sigma_{d2} = -\int_0^h \rho_e dy, \tag{13}$$

As long as $\sigma_{d1} + \sigma_{d2} \neq 0$, Eq. (13) and Eq. (11) can replace Eq. (10) to provide two relations among σ_{d1}, ζ_1, σ_{d2}, and ζ_2.

As an example, for 1:1 electrolyte with Debye-Hückel approximation, the two electrostatic equilibrium conditions can be obtained by combining Eq. (8) and Eq. (10) [78],

$$\sigma_{d1} = \kappa\varepsilon_0\varepsilon_r(\sinh\kappa h)^{-1}(\zeta_1\cosh\kappa h - \zeta_2), \tag{14}$$

$$\sigma_{d2} = \kappa\varepsilon_0\varepsilon_r(\sinh\kappa h)^{-1}(\zeta_2\cosh\kappa h - \zeta_1), \tag{15}$$

3.3. Charging of rock-brine interface

3.3.1. Sandstone-brine interfaces

Sandstone-brine interface is typically negatively charged. Silica is the most common mineral in sandstone reservoirs. Basic Stern (BS) model assumes silica is negatively charged due to dissolution of silanol groups [79]:

$$>\mathrm{SiOH} \rightleftharpoons >\mathrm{SiO^-} + \mathrm{H^+},\ K_{a2}^{\mathrm{int}} \tag{16}$$

where the greater-than symbols are used to differentiate surface groups from single molecules and ions. The dissolution constant K_{a2}^{int} is expressed as:

$$K_{a2}^{\mathrm{int}} = 10^{-pK} = c_{\mathrm{H^+}}^\infty\exp(-\psi_0)\Gamma_{>\mathrm{SiO^-}}/\Gamma_{>\mathrm{SiOH}}, \tag{17}$$

where $\Gamma_{>SiO^-}$ and $\Gamma_{>SiOH}$ are respectively the surface density of $>SiO^-$ and $>SiOH$, and $\psi_0 = e\phi_0/k_bT$ is the dimensionless surface potential. Then the surface charge density can be expressed as

$$\sigma_0 = -e\Gamma_{>\mathrm{SiO^-}}. \tag{18}$$

Due to mass conservation,

$$\Gamma_0 = \Gamma_{>\mathrm{SiO^-}} + \Gamma_{>\mathrm{SiOH}}. \tag{19}$$

In addition, ϕ_0, σ_0, and ζ can be related by

$$\mathbf{C} = \sigma_0/(\phi_0 - \zeta), \tag{20}$$

where $\mathbf{C}$ is the phenomenological capacity of the Stern layer. With the approximation $\sigma_0 \approx \sigma_d$, Eq.(17)-(20) lead to

$$\psi_d = \ln\frac{-\sigma_d}{e\Gamma_0 + \sigma_d} - (\mathrm{pH} - \mathrm{pK})\ln 10 - \frac{\sigma_d e}{\mathbf{C}k_bT}. \tag{21}$$

$\Gamma_0 = 8\ nm^{-2}$, $\mathrm{pK} = 7.5$, and $\mathbf{C} = 2.9\ \mathrm{F}\ m^{-2}$ are suggested by Ref. [79]. The combination of Eq. (21) and the Grahame equation (Eq. (12)) determines σ_d and ψ_d for an isolated brine-silica interface.

Basic Stern model is only applicable to very dilute solutions [79,80], while brine used in IDF usually has the ionic strength higher than 0.01 M. It should be better to use electrical triple-layer (ETL) model [80–82] to predict silica surface charge for a broad range of ionic concentration. Sketch of ETL model is shown in Fig. 4. In addition to Eq. (16), ETL model also considers the surface complexation of salt ions:

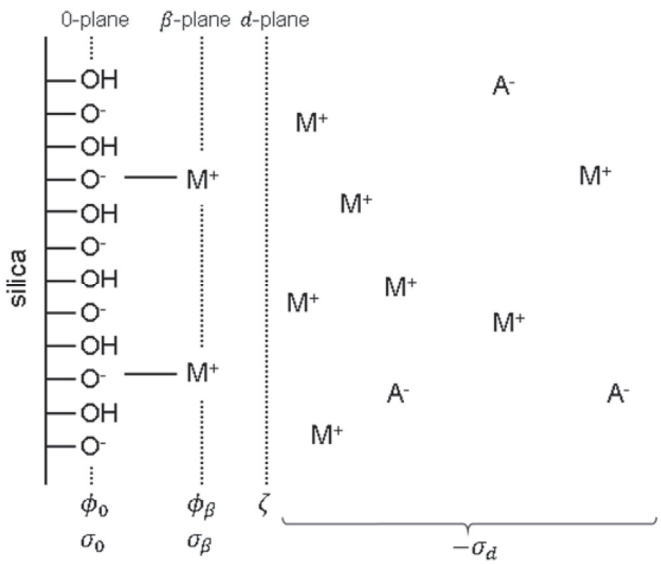

Fig. 4. A sketch of ETL model, assuming monovalent cations. The symbols M^+ and A^- represent metal cations and anions in the solution. ϕ_0 and σ_0 are respectively surface potential and surface charge density, ϕ_β and σ_β are respectively electrical potential and charge density of Stern layer, ζ is the electrical potential of the slip plane and σ_d is the equivalent surface charge density.

$$>SiO^- + M^{z+} \rightleftharpoons >SiOM^{(z-1)+}, \quad K_M^{int}. \tag{22}$$

The adsorption equilibrium constant K_M^{int} satisfies:

$$K_M^{int} = \Gamma_{>SiOM^{(z-1)+}} \exp\left(z\psi_\beta\right) \Big/ c_{M^{z+}}^{\infty} \Gamma_{>SiO^-}, \tag{23}$$

where $\psi_\beta = e\phi_\beta/k_bT$ is the dimensionless electrical potential of the Stern layer. Similar to the BS model, the following equations must be satisfied:

$$\Gamma_0 = \Gamma_{>SiO^-} + \Gamma_{>SiOH} + \Gamma_{>SiOM^{(z-1)+}}, \tag{24}$$

$$\sigma_0 = -e(\Gamma_{>SiO^-} + \Gamma_{>SiOM^{(z-1)+}}), \tag{25}$$

$$\sigma_\beta = ze\Gamma_{>SiOM^{(z-1)+}}, \tag{26}$$

$$\sigma_d = \sigma_0 + \sigma_\beta, \tag{27}$$

$$\phi_0 - \phi_\beta = \sigma_0/\mathbf{C}_1, \tag{28}$$

$$\phi_\beta - \zeta = -\sigma_d/\mathbf{C}_2, \tag{29}$$

where $\mathbf{C}_1$ and $\mathbf{C}_2$ are the integral electrical capacities of the inner and outer parts of the Stern layer, and σ_0, σ_d, σ_β, ϕ_0, ϕ_β and ζ are illustrated in Fig. 4. ETL model combined with the Grahame equation (Eq. (12)) determine the surface charging quantities for a single EDL. The ETL model is well consistent with experiments for amorphous silica/quartz-NaCl (aq) system [80,81].

In regard to the charging of more complex minerals in sandstones, such as Kaolinite, there are more charging complexations besides that described by Eqs. (16) and (22). Readers can refer to [24] for more information.

3.3.2. Carbonate-brine interface

When it comes to the carbonate-brine interface, the charging mechanism is much more complex. Take calcite ($CaCO_3$) as an example [83–87]. Calcite can be partially dissolved in water, so the water interacting with calcite must at least contain Ca^{2+}, CO_3^{2-}, HCO_3^-, H^+ and OH^-. The hydration of the calcite surface in water produces two types of surface sites: $>CaOH$ and $>CO_3H$, similar to the $>SiOH$ on silica. $>CaOH$ and $>CO_3H$ can act with the H^+ and OH^- in water,

$$>CO_3H \rightleftharpoons >CO_3^- + H^+, \tag{30}$$

$$>CaOH \rightleftharpoons >CaO^- + H^+, \tag{31}$$

$$>CaOH + H^+ \rightleftharpoons >CaOH_2^+. \tag{32}$$

The $>CO_3H$ can further attract the Ca^{2+} in water,

$$>CO_3H + Ca^{2+} \rightleftharpoons >CO_3Ca^+ + H^+. \tag{33}$$

In addition, the $>CaOH$ can react with the dissolved CO_2,

$$>CaOH + CO_2 \rightleftharpoons >CaHCO_3, \tag{34}$$

$$>CaOH + CO_2 \rightleftharpoons >CaCO_3^- + H^+, \tag{35}$$

Therefore the pressure of CO_2 influences the charging of calcite as well. The reaction constants of Eq.(30)-(35) can be referred to [83–85]. The total number of surface sites should be constant:

$$\Gamma_0 = \Gamma_{>CO_3H} + \Gamma_{>CaOH} + \Gamma_{>CO_3^-} + \Gamma_{>CaO^-} + \Gamma_{>CaOH_2^+} + \Gamma_{>CO_3Ca^+} + \Gamma_{>CaHCO_3} + \Gamma_{>CaCO_3^-}, \tag{36}$$

and Γ_0 is recommended as 2 or 5 nm^{-2}. The surface charge density of the calcite-brine interface can be expressed as:

$$\sigma_0 = e\left(-\Gamma_{>CO_3^-} - \Gamma_{>CaO^-} + \Gamma_{>CaOH_2^+} + \Gamma_{>CO_3Ca^+} - \Gamma_{>CaCO_3^-}\right). \tag{37}$$

$\sigma_0 \approx \sigma_d$ and $\phi_0 \approx \zeta$ are usually assumed, so the combination of the above equations with the Grahame equation can determine the charging quantities of an isolated calcite-water interface.

When other salts are added to the water, the charging of calcite can be even more complexed. The adding of 1:1 electrolyte generally does not contribute to additional charging mechanisms, and its effects are only reflected in the Grahame equation. In contrast, the adding of Ca^{2+} can influence the reaction equilibrium of Eq. (33); the adding of Mg^{2+} can produce a new reaction similar to Eq. (33); the adding of SO_4^{2-} can cause [84,85]:

$$>CaOH_2^+ + SO_4^{2-} \rightleftharpoons >CaSO_4^- + H_2O, \tag{38}$$

which reaction can make calcite negatively charged with sufficient SO_4^{2-}. Using the reactions described by Eq.(30)–(35) and (38), Hiorth et al. [84] successfully predicted the zeta potential measured by various researchers.

3.4. Charging of oil-brine interface

3.4.1. Nonpolar oil-brine interface

Nonpolar oil is widely used to study OBR interaction instead of crude oil since it can provide more repeatable experimental data. Unlike polar oil or rock, nonpolar oil does not have ionizable sites. Marinova et al. [69] summarized several possible charging mechanisms: (1) the adsorption of hydroxyls; (2) the adsorption of other anions such as Cl^-; (3) the desorption of H^+; (4) the orientation of

water molecules; (5) adsorption of some contaminations. However, which mechanism dominates is still under debate [70,88–90].

In the following, we just introduce the hydroxyl adsorption mechanism. Marinova et al. [69] proposed that the charging of nonpolar oil-brine interface is independent on the oil type, and hydroxyl ions adsorption should be the main charging mechanism. They assumed $\sigma_0 \approx \sigma_d$ and $\phi_0 \approx \zeta$, and used Stern isotherm to describe the ion adsorption:

$$\Gamma = -\frac{\sigma_0}{e} = \frac{\Gamma_0 v_0 N_A c^{\infty}_{OH^-} \exp(-(\Phi - e\zeta)/k_b T)}{1 + v_0 N_A c^{\infty}_{OH^-} \exp(-(\Phi - e\zeta)/k_b T)}, \tag{39}$$

where Γ_0 is the saturation adsorption, $v_0 = 1.1 \times 10^{-22}\ cm^{-3}$ is the volume of a hydrated hydroxyl ion in solution, and Φ is a constant. Γ_0 and Φ can be varied to fit experimental data. The combination of Eq. (39) and the Grahame equation determines σ_d and ζ of single nonpolar oil-brine interface. Marinova et al. [69] used $\Gamma_0 = 9.8 \times 10^{-8}\ mol\ m^{-2}$ and $\Phi = -25 k_b T$, and found good agreement between theory and experiment for xylene-NaCl (aq) interface.

3.4.2. Polar oil-brine interface

The polar groups of the oil tend to move to the oil-brine interface, and some of them can get ionized in contact with water, causing the charging of the interface. This mechanism is usually named as ionization of surface groups (ISG). A typical description is given by Buckley et al. [47]. They supposed that crude oil-brine interface is charged due to the deprotonation of acid groups >AH and the protonation of basic groups >B:

$$>AH \rightleftharpoons >A^- + H^+,\ \ K_a, \tag{40}$$

$$>BH^+ \rightleftharpoons >B + H^+,\ \ K_b. \tag{41}$$

The reaction constants satisfy:

$$K_a = (\Gamma_{>A^-}/\Gamma_{>AH}) c^{\infty}_{H^+} \exp(-\psi_0), \tag{42}$$

$$K_b = (\Gamma_{>B}/\Gamma_{>BH^+}) c^{\infty}_{H^+} \exp(-\psi_0). \tag{43}$$

Then the surface charge density can be described as

$$\sigma_0 = e(\Gamma_{>BH^+} - \Gamma_{>A^-}). \tag{44}$$

In addition, due to mass conservation,

$$\Gamma_a = \Gamma_{>A^-} + \Gamma_{>AH}, \tag{45}$$

$$\Gamma_b = \Gamma_{>B} + \Gamma_{>BH^+}, \tag{46}$$

where Γ_a and Γ_b are respectively the surface density of all the acid and basic groups. The combination of Eq.(42)-(46) leads to

$$\sigma_0 = e\Gamma_b \left(1 + (K_b/c^{\infty}_{H^+}) \exp(\psi_0)\right)^{-1} - e\Gamma_a \left(1 + (c^{\infty}_{H^+}/K_a) \exp(-\psi_0)\right)^{-1}. \tag{47}$$

Buckley et al. [47] assumes $\sigma_0 \approx \sigma_d$, both the Stern layer and the diffuse layer satisfy the PB equation, and the slip plane is located a distance 0.6 nm from the surface, to determine ζ. They also provided the constants for Leduc, ST-86-1, and Moutray crude oil that make the model well consistent with experiments for crude oil-NaCl (aq) system.

3.5. Discussion: boundary conditions for two interacting EDLs

For one single EDL, the Grahame equation and the charging model respectively provide one implicit or explicit relation between ζ and σ_d. Combination of the two relations determines ζ and σ_d. For two interacting EDLs, interface charging quantities can influence each other especially at short distances, which phenomena is called charge regulation (CR). The CR boundary is usually complex to solve. Two relations among ζ_1, ζ_2, σ_{d1}, and σ_{d2} are given by the general electrostatic equilibrium conditions. One relation between ζ_1 and σ_{d1} and one relation between ζ_2 and σ_{d2} are respectively given by the charging models of the two interfaces. The four relations need to be solved to give ζ_1, ζ_2, σ_{d1}, and σ_{d2}. To simplify the problem, constant charge (CC) or constant potential (CP) assumption is commonly used, to replace the two relations given by charging models for two interacting EDLs. However, near contact line the rock-brine and brine-oil interfaces are so close that the CC and CP boundaries may bring large error. In the following, we will discuss how ζ_1, ζ_2, σ_{d1}, and σ_{d2} change with h for the three boundary conditions, to see the limitations of CC and CP boundaries.

For the CC boundary, the total charge of brine should be finite, thus $d\phi/dy$ should also be finite according to the integration of the PB equation. Therefore, ϕ becomes uniform between two interfaces when $h \to 0$. Then, based on Eq. (13), we can know that

$$h \to 0:\ \zeta_1 \to \zeta,\ \zeta_2 \to \zeta,\ \text{where } \zeta \text{ satisfies } \sigma_{d1} + \sigma_{d2} = -h \sum_i z_i e n_i^{\infty} \exp(-z_i e\zeta/k_b T)\ \ (\text{constant charge}). \tag{48}$$

Based on Eq. (48), as $h \to 0$, if $\sigma_{d1} + \sigma_{d2} = 0$, ζ_1, $\zeta_2 \to 0$; if $\sigma_{d1} + \sigma_{d2} > 0$, then ζ_1, $\zeta_2 \to +\infty$; and if $\sigma_{d1} + \sigma_{d2} < 0$, then ζ_1, $\zeta_2 \to -\infty$. That is, the CC boundary can lead to unphysical zeta potential on the two interfaces if $\sigma_{d1} + \sigma_{d2} \neq 0$. The analysis is consistent with that predicted by full PB equation, as shown in Fig. 5(a).

For the CP boundary, ϕ in the water film should be finite, thus $d^2\phi/dy^2$ should also be finite based on the PB equation. Therefore, when $h \to 0$, $d\phi/dy$ should be a constant independent on location. Then, based on Eq. (10), we can know that

$$h \to 0:\ \ \sigma_{d1} \to \varepsilon_r \varepsilon_0 (\zeta_1 - \zeta_2)/h,\ \ \sigma_{d2} \to \varepsilon_r \varepsilon_0 (\zeta_2 - \zeta_1)/h\ \ (\text{constant potential}). \tag{49}$$

Based on Eq. (49), as $h \to 0$, if $\zeta_1 = \zeta_2$, then $\sigma_{d1}, \sigma_{d2} \to 0$; if $\zeta_1 > \zeta_2$, then $\sigma_{d1} \to +\infty$ and $\sigma_{d2} \to -\infty$; and if $\zeta_1 < \zeta_2$, then $\sigma_{d1} \to -\infty$ and $\sigma_{d2} \to +\infty$. That is, the CP boundary can lead to unphysical surface charge densities for asymmetrical interfaces ($\zeta_1 \neq \zeta_2$). The analysis is consistent with that predicted by the full PB equation, as shown in Fig. 5(b).

For the CR boundary, the charging models limit the magnitude of σ_{d1} and σ_{d2} by the number of total possible site charges, and we assume $\alpha_1 = \min(\sigma_{d1})$, $\beta_1 = \max(\sigma_{d1})$, $\alpha_2 = \min(\sigma_{d2})$, and $\beta_2 = \max(\sigma_{d2})$. Usually $\alpha_1, \alpha_2 \le 0$ and $\beta_1, \beta_2 \ge 0$. Since σ_{d1} and σ_{d2} are finite, from PB equation, Eq. (48) is also valid for the CR boundary as $h \to 0$. Actually the charging models can be combined with Eq. (48) to further restrict the relation, respectively for the following four conditions. (1) $\alpha_1 + \alpha_2 < 0$ and $\beta_1 + \beta_2 > 0$. In this case, the two interfaces can be oppositely charged. If $\zeta \to +\infty$, based on charging models, the positive potential determining ions are all expelled from the water film while the negative potential determining ions are attracted to the water film, and so $\sigma_{d1} + \sigma_{d2} < 0$. This is contradicted with Eq. (48). Similarly it can be inferred that ζ cannot be infinitely negative. Therefore, ζ must be

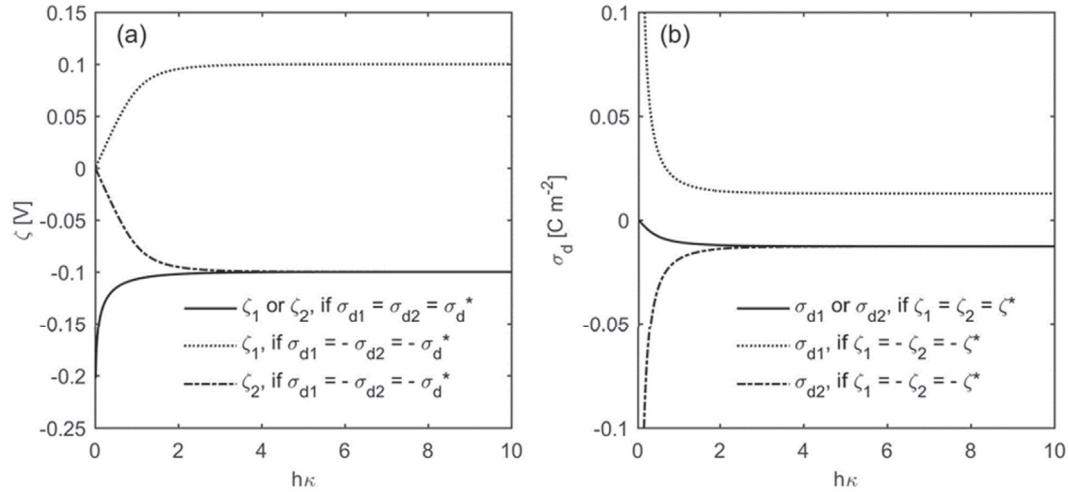

Fig. 5. The interface charging quantities along with the dimensionless water film thickness $h\kappa$ at 298 K for (a) the constant charge (CC) boundary and (b) the constant potential (CP) boundary. The electrolyte is 1:1 with bulk concentration 0.001 M $\zeta^* = -0.1$ V, and σ_d^* satisfies the same Grahame equation (Eq. (12)) with ζ^*.

finite, and Eq. (48) indicates that $\sigma_{d1} + \sigma_{d2} \to 0$ as $h \to 0$. (2) $\alpha_1 = \alpha_2 = 0$ and $\beta_1 + \beta_2 > 0$. In this case, $\sigma_{d1} + \sigma_{d2} \geq 0$, so $\zeta \geq 0$ based on Eq. (48). Besides, if ζ is finitely positive, based on the charging models, $\sigma_{d1} + \sigma_{d2} > 0$, which is contradicted with Eq. (48). Therefore, $\zeta \to +\infty$ and $\sigma_{d1}, \sigma_{d2} \to 0$. (3) $\alpha_1 + \alpha_2 < 0$ and $\beta_1 = \beta_2 = 0$. Similarly analyzed as case (2), $\zeta \to -\infty$ and $\sigma_{d1}, \sigma_{d2} \to 0$. (4) $\alpha_1 = \alpha_2 = 0$ and $\beta_1 = \beta_2 = 0$, neither of the interfaces is charged, so $\sigma_{d1} + \sigma_{d2} = 0$. The common behaviors of the above four cases are,

$$h \to 0: \ \zeta_1 - \zeta_2 \to 0, \ \alpha_1 \leq \sigma_{d1} \leq \beta_1, \ \alpha_2 \leq \sigma_{d2} \leq \beta_2, \ \text{and} \ \sigma_{d1} + \sigma_{d2} \to 0 \quad (\text{charge regulation}). \tag{50}$$

Eq.(48)-(50) can also indicate that the CR boundary leads to less extreme ζ_1, ζ_2 compared with the CC boundary, and less extreme σ_{d1}, σ_{d2} compared with the CP boundary. We will take two polar oil-NaCl (aq)-silica systems as two examples to show the convergence of the boundaries as $h \to 0$, as discussed in Sec. 3.6.

The above analysis will be very useful to judge the effectivity to calculate EDL interaction energy with different boundary conditions for two interacting EDLs, as shown in Sec. 4.2.2.

3.6. Case analysis: polar oil-NaCl (aq)-silica system

We would like to select two systems for case analysis, in one of which oil and rock are oppositely charged and in the other oil and rock are similarly charged. For this, we use the ISG model for polar oil, taking the parameters K_a and K_b from Ref. [47] for crude oil ST-86-1, and change Γ_a and Γ_b to produce one positively charged oil (oil P) and one negatively charged oil (oil N). When using the ISG model, the approximations $\sigma_0 \approx \sigma_d$ and $\phi_0 \approx \zeta$ are used. The two oils can respectively form the required systems with amorphous silica and NaCl solution. We use the ETL model for the amorphous silica-NaCl (aq) interface, taking parameters from literature [81]. In the following, we will simply refer to amorphous silica as silica.

First, the zeta potential for single EDL with different ionic composition is calculated, to present an overview of how silica, oil N, and oil P are charged, as shown in Fig. 6. Basically silica-NaCl (aq) interface and oil N-NaCl (aq) interface are more negatively charged for higher pH and lower concentration, and oil P-NaCl (aq) interface is more positively charged for smaller pH and lower concentration. These values of zeta potential will be used in the following sections to analyze EDL interaction energy and ion-tuned wettability.

Next, the charging quantities of these two OBR systems along

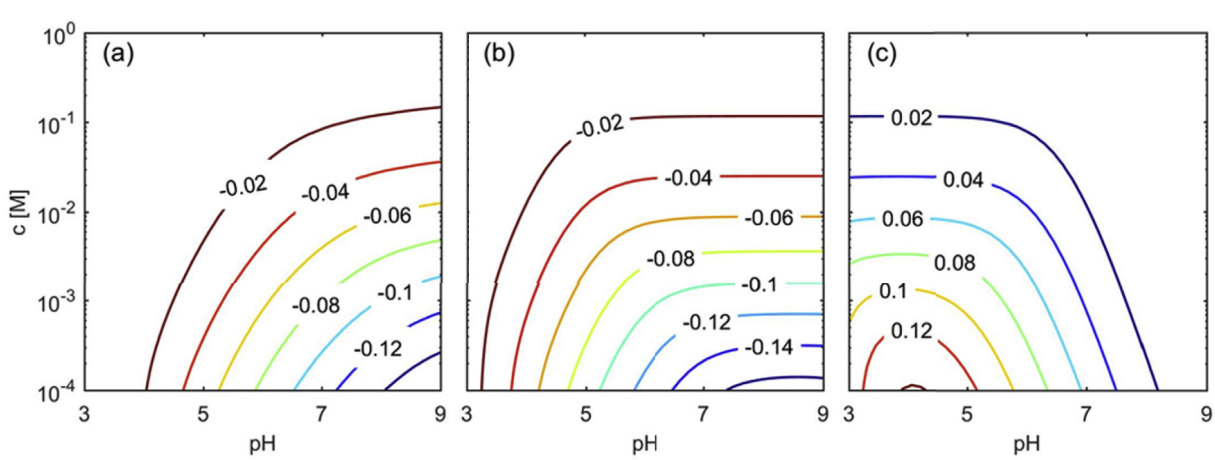

Fig. 6. The zeta potential (unit: V) of (a) amorphous silica, (b) oil N, and (c) oil P immersed in NaCl solution, for different ionic composition at 298 K. The ETL model parameters for amorphous silica are $\Gamma_0 = 5\ nm^{-2}$, $\mathbf{C}_1 = 1.25\ \mathrm{F}\ m^{-2}$, $\mathbf{C}_2 = 0.20\ \mathrm{F}\ m^{-2}$, $\lg K_{a2}^{\mathrm{int}} = -6.73$, and $\lg K_{\mathrm{Na}}^{\mathrm{int}} = -0.25$. The ISG model parameters for polar oil are $\lg K_a = -4$, $\lg K_b = -7$, and $\Gamma_a + \Gamma_b = 0.1\ nm^{-2}$; for polar oil P $\Gamma_a = 0$ and for polar oil N $\Gamma_b = 0$.

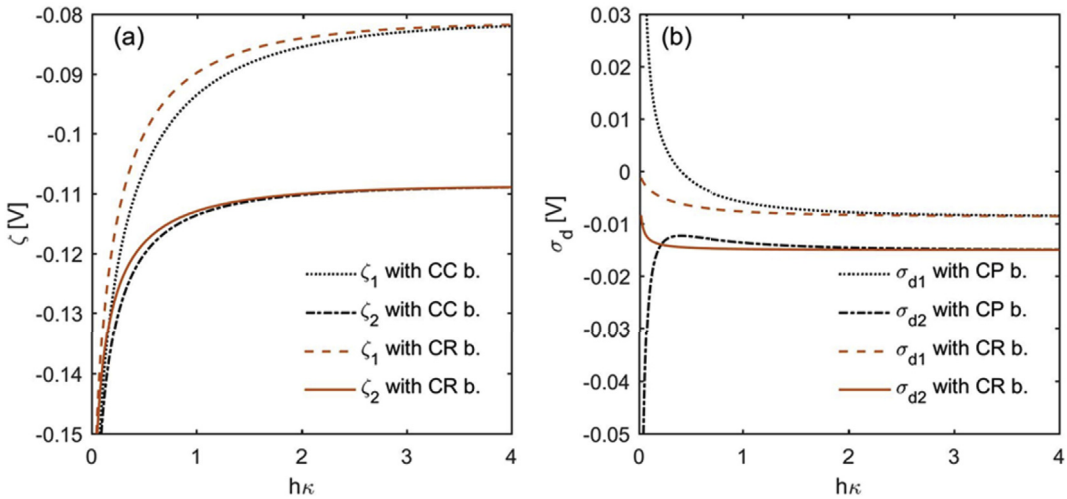

Fig. 7. (a) The zeta potential and (b) the equivalent surface charge density along with the dimensionless water film thickness $h\kappa$ in oil N-NaCl (aq)-silica system at 298 K. The NaCl bulk concentration is 0.001 M, and the pH is 7.

with the dimensionless water film thickness $h\kappa$, using different boundary conditions, are shown in Fig. 7 and Fig. 8. The results are consistent with the analysis in Sec. 3.5. With the CR boundary, as $h \to 0$, ζ_1 and ζ_2 tend to identical, σ_{d1} and σ_{d2} are always finite and $\sigma_{d1} + \sigma_{d2} \to 0$. The CC and CP boundaries deviate from the CR boundary when $h\kappa < 3$, and lead to extreme charging quantities when $h\kappa < 0.1$. The CC boundary overestimates the magnitude of ζ_1 and ζ_2 because it overestimates the magnitude of $\sigma_{d1} + \sigma_{d2}$. The CP boundary leads to infinite σ_{d1} and σ_{d2} as $h \to 0$, which is apparently unphysical.

4. The energy of EDL interaction

In this section, we aim to introduce how to calculate the energy of EDL interaction. Firstly, in Sec. 4.1, three methods to derive the EDL interaction energy will be introduced, and the expressions for the CR, CC, and CP boundaries, if existed, will be presented for each method. Next two issues will be discussed in Sec. 4.2: the unity of the three methods, and the convergence analysis for different boundaries. Finally, the two typical OBR systems, which have been presented in Sec. 3.6, are taken as examples to analyze the EDL interaction energy in Sec. 4.3.

4.1. Methods to derive the EDL interaction energy

Verwey and Overbeek [76] described three methods to calculate the EDL interaction energy in the system as shown in Fig. 3. Two methods assume reversible processes to calculate the free energy of the two interacting EDLs, which is denoted as F, and then get the EDL interaction energy by

$$w_{EDL} = F(h) - F(\infty), \tag{51}$$

Depending on the assumed reversible processes to calculate free energy, we refer to these two methods as surface charging method and electrolyte discharging method. The third method, which we refer to as pressure integrating method, uses thermodynamic relations to analyze the pressure between two charged interfaces Π_{EDL}, then integrate the pressure to get the EDL interaction energy:

$$w_{EDL} = \int_h^\infty \Pi_{EDL} \mathrm{d}h. \tag{52}$$

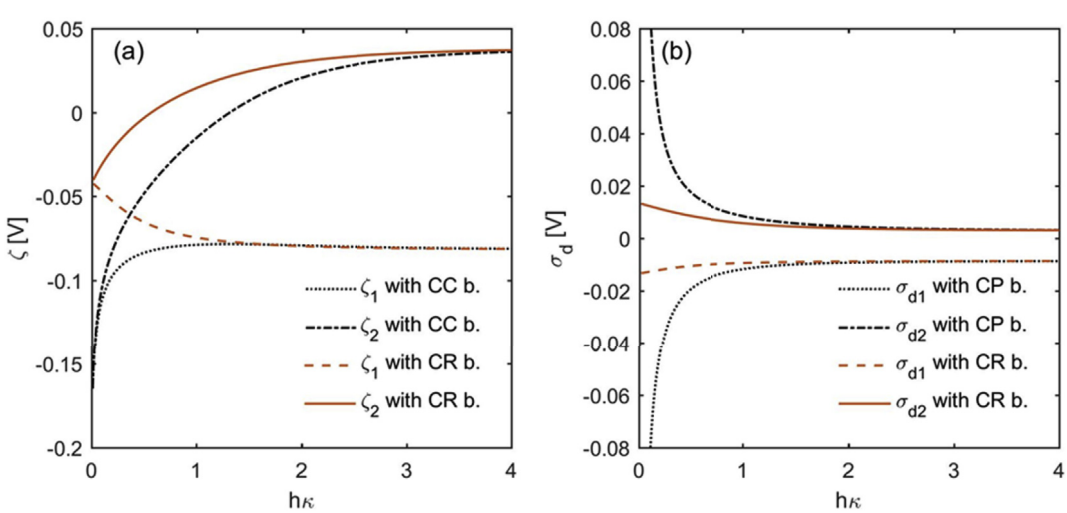

Fig. 8. (a) The zeta potential and (b) the equivalent surface charge density along with the dimensionless water film thickness $h\kappa$ in oil P-NaCl (aq)-silica system at 298 K. The NaCl bulk concentration is 0.001 M, and the pH is 7.

We will introduce the three methods in this section, mainly based on [76] but also including the important complements from other researchers.

4.1.1. Surface charging method

In this method, the EDL is imagined to form by the following reversible, isometric and isothermal process. First an infinitely small amount of potential determining ions are adsorbed to or desorbed from the interface, and then the ions in brine rearrange their positions to the balance of diffusion and Coulombic forces. These two steps go after each other until the complete ionic equilibrium has reached. Free energy obtained in one adsorbing/desorbing step for a single EDL is:

$$\mathrm{d}F = \sum_j \left(\mu_j^S - \mu_j^\infty\right)\mathrm{d}\Gamma_j, \tag{53}$$

where μ_j^S and μ_j^∞ are respectively the electrochemical potential for the j-th type of potential determining ions at the interface and the bulk solution, and $\mathrm{d}\Gamma_j$ is the amount of adsorbed j-th type of ions per unit surface area in this step (negative for desorbing process). During the diffusion steps, for each ion in brine, the electrical energy gained from the interface charge is all spent on diffusion. Thus the electrochemical potential for these ions does not change during the whole reversible process, resulting that the diffusion steps do not contribute any free energy change.

In the following, we first derive the free energy for one single EDL. We neglect the Stern layer, so $\sigma_0 \approx \sigma_d$ and $\phi_0 \approx \zeta$. The surface density during the charging process can be expressed as

$$\sigma'_0 = \sum_j z_j e \Gamma_j, \tag{54}$$

where the apostrophes mark quantities in the surface charging process, to distinguish them from those at final equilibrium state. According to classical thermodynamics,

$$\mu_j^S = \overline{\mu}_j^S + z_j e \phi_0^e(\sigma'_0), \tag{55}$$

where ϕ_0^e represents the interface potential which satisfies the Grahame equation when the interface bears charge σ'_0, while $\overline{\mu}_j^S$ and $z_i e \phi_0^e$ are respectively the chemical and electrical potential part of μ_j^S. Based on Eq.(53)-(55), the free energy can be divided into two parts: the electrical part

$$F_{\mathrm{elec}} = \int_0^{\sigma_0} \phi_0^e(\sigma'_0)\mathrm{d}\sigma'_0, \tag{56}$$

and the chemical part

$$F_{\mathrm{chem}} = \int_0^{\sigma_0} \left(\overline{\mu}_j^S - \mu_j^\infty\right)\mathrm{d}\sigma'_0. \tag{57}$$

F_{elec} can be easily calculated based on the Grahame equation, while we need to do more work on F_{chem}. Assume the electrolyte as ideal solution,

$$\overline{\mu}_j^S = \mu_j^0 + k_b T \ln c_j^S, \tag{58}$$

where μ_j^0 is the standard chemical potential, c_j^S is the concentration of j-th type of potential determining ions at the interface. From the charging models, we can obtain another interface potential $\phi_0^c(\sigma'_0)$, as discussed in Sec. 3.5. $\phi_0^c(\sigma_0')$ relates the c_j^S with the bulk concentration c_j^∞ by Boltzmann equation, thus

$$\overline{\mu}_j^S = \mu_j^0 + k_b T \ln c_j^\infty - z_j e \phi_0^c(\sigma'_0) = \mu_j^\infty - z_j e \phi_0^c(\sigma'_0). \tag{59}$$

Note that $\phi_0^c \neq \phi_0^e$ unless σ'_0 reaches the equilibrium value σ_0, since there is only one common solution of the Grahame equation and charging models. Based on Eq.(58)-(59), Eq. (57) can be written as [91,92].

$$F_{\mathrm{chem}} = -\int_0^{\sigma_0} \phi_0^c(\sigma'_0)\mathrm{d}\sigma'_0, \tag{60}$$

which is a relatively generalized expression for F_{chem}.

Similarly, we can derive the free energy for two interacting EDLs,

$$F_{\mathrm{elec}}(h) = \int_{(0,0)}^{(\sigma_{01}(h),\sigma_{02}(h))} \phi_{01}^e(\sigma'_{01},\sigma'_{02},h)d\sigma'_{01} + \phi_{02}^e(\sigma'_{01},\sigma'_{02},h)d\sigma'_{02}, \tag{61}$$

where the functions $\phi_{01}^e(\sigma'_{01}, \sigma'_{02}, h)$ and $\phi_{01}^e(\sigma'_{01}, \sigma'_{02}, h)$ are obtained from the electrostatic equilibrium conditions combined with the PB equation, and

$$F_{\mathrm{chem}}(h) = -\int_{(0,0)}^{(\sigma_{01}(h),\sigma_{02}(h))} \phi_{01}^c(\sigma'_{01})d\sigma'_{01} + \phi_{02}^c(\sigma'_{02})d\sigma'_{02}. \tag{62}$$

where $\phi_{01}^c(\sigma'_{01})$ and $\phi_{02}^c(\sigma'_{02})$ are obtained from the charging models. The integration is independent on path. Then the EDL interaction energy can be obtained by Eq. (51). We refer to the EDL interaction obtained from the exact solution of the EDL charge regulation model and Eq. (61) as the charge regulation (CR) solution. However, $\phi_{01}^c(\sigma'_{01})$ and $\phi_{02}^c(\sigma'_{02})$ can be very complicated when the charging models involve multi reactions and capacitances. Therefore, the constant charge (CC) and constant potential (CP) boundaries may be used to replace the charging models. If the CC boundary is assumed, then $F_{\mathrm{chem}}(h) - F_{\mathrm{chem}}(\infty)$ can be neglected, and

$$\begin{aligned} w_{EDL} &= F_{\mathrm{elec}}(h) - F_{\mathrm{elec}}(\infty) \\ &= \int_{(0,0)}^{(\sigma_{01},\sigma_{02})} \left(\phi_{01}^e(\sigma'_{01},\sigma'_{02},h) - \phi_{01}^e(\sigma'_{01},\sigma'_{02},\infty)\right)d\sigma'_{01} \\ &\quad + \left(\phi_{02}^e(\sigma'_{01},\sigma'_{02},h) - \phi_{02}^e(\sigma'_{01},\sigma'_{02},\infty)\right)d\sigma'_{02} \\ &\quad (\text{constant charge}). \end{aligned} \tag{63}$$

If the CP boundary is assumed [91], then $\phi_{01}^c = \phi_{01}$, and $\phi_{02}^c = \phi_{02}$, so we rewrite F_{chem} as

$$F_{\mathrm{chem}}(h) = -\sigma_{01}(h)\phi_{01} - \sigma_{02}(h)\phi_{02}, \tag{64}$$

and then

$$w_{EDL} = -\int_{(0,0)}^{(\phi_{01},\phi_{02})} \left(\sigma'_{01}(\phi^e_{01},\phi^e_{02},h) - \sigma'_{01}(\phi^e_{01},\phi^e_{02},\infty)\right) d\phi^e_{01} + \left(\sigma'_{02}(\phi^e_{01},\phi^e_{02},h) - \sigma'_{02}(\phi^e_{01},\phi^e_{02},\infty)\right) d\phi^e_{02} \quad \text{(constant potential)}. \tag{65}$$

where the functions $\sigma'_{01}(\phi^e_{01},\phi^e_{01},h)$ and $\sigma'_{02}(\phi^e_{01},\phi^e_{01},h)$ come from the electrostatic equilibrium conditions combined with the PB equation. For a 1:1 electrolyte with Debye-Hückel linear approximation, Eq.(14)-(15) can be applied into Eq. (65), and then [78]:

$$w_{EDL} = \kappa\varepsilon_0\varepsilon_r(2\sinh\kappa h)^{-1}\left(2\zeta_1\zeta_2 + \left(\zeta_1^2+\zeta_2^2\right)(\sinh\kappa h - \cosh\kappa h)\right) \quad \text{(HFF equation)}, \tag{66}$$

which is named Hogg-Healy-Fuerstenau (HHF) equation [56], and is widely used to describe the EDL repulsion between asymmetrical interfaces. Buckley et al. [47] used the HHF equation to analyze the effect of electrical charges on oil adhesion to silica, and found its good agreement with experiments. Hirasaki [46] also suggested the HHF equation to calculate contribution of EDL repulsion to contact angle variation. However, HHF equation cannot deal with multivalent ions and large zeta potentials, which may occur in OBR systems, and its constant potential assumption may also lead to unphysical EDL interaction energy at small h, as discussed in Sec. 4.2.2.

4.1.2. Electrolyte discharging method

The main idea of the electrolyte discharging method is analogous to the theory of strong electrolytes by Debye and Hückel. The following reversible, isometric and isothermal process is suggested: in the first step, part of the charge of each ion $z_i e d\lambda$ is moved to infinity; in the second step, ions arrange themselves due to balance between diffusion and electrical field; then these two steps go after each other until each ion is neutral. Free energy is only dismissed in the discharging steps. In the first step the free energy assumption in dV is

$$\sum_i \phi' z_i e \mathrm{d}\lambda \cdot n_i \mathrm{d}V = \phi' \mathrm{d}\lambda \mathrm{d}V \sum_i z_i e n_i = \phi' \rho'_e \mathrm{d}\lambda \mathrm{d}V/\lambda, \tag{67}$$

where ϕ' and ρ'_e represent local electrical potential and volume charge density during electrolyte discharging. Thus the free energy can be expressed as:

$$F = \int_0^1 \frac{d\lambda}{\lambda} \iiint \rho'_e \phi' dV, \tag{68}$$

which can be used for both a single EDL and two interacting EDLs, and can easily deal with complex interface topologies. It is obvious that

$$\phi' \mathrm{d}\lambda = \frac{\partial}{\partial\lambda}(\lambda\phi')\mathrm{d}\lambda - \lambda\frac{\partial\phi'}{\partial\lambda}\mathrm{d}\lambda. \tag{69}$$

For the EDLs between two parallel charged plates, based on the PB equation,

$$\rho'_e = -\varepsilon_0\varepsilon_r\frac{\partial^2\phi'}{\partial y^2} = \sum_i \lambda z_i e n_i^\infty \exp(-\lambda z_i e\phi'/k_bT) = -k_bT\lambda\frac{\partial}{\partial(\lambda\phi')}\sum_i n_i^\infty \exp(-\lambda z_i e\phi'/k_bT). \tag{70}$$

Substitute Eq.(69)-(70) into Eq. (68), then

$$\begin{aligned} F_h &= \int_0^1 \frac{\mathrm{d}\lambda}{\lambda}\int_0^h \rho'_e\phi' \mathrm{d}y \\ &= -k_bT\int_0^1\int_0^h \frac{\partial(\lambda\phi')}{\partial\lambda}\frac{\partial}{\partial(\lambda\phi')}\sum_i n_i^\infty \exp(-\lambda z_i e\phi'/k_bT)\mathrm{d}y\mathrm{d}\lambda \\ &\quad + \varepsilon_0\varepsilon_r\int_0^1\int_0^h \frac{\partial\phi'}{\partial\lambda}\frac{\partial^2\phi'}{\partial y^2}\mathrm{d}y\mathrm{d}\lambda \\ &= -k_bT\int_0^h\left(\sum_i n_i - \sum_i n_i^\infty\right)\mathrm{d}y - \frac{\varepsilon_0\varepsilon_r}{2}\int_0^h\left(\frac{\mathrm{d}\phi}{\mathrm{d}y}\right)^2\mathrm{d}y \\ &\quad + \varepsilon_0\varepsilon_r\int_0^1\left(\frac{\partial\phi'}{\partial y}\frac{\partial\phi'}{\partial\lambda}\right)\Big|_{y=0}^{y=h}\mathrm{d}\lambda, \end{aligned} \tag{71}$$

Assume $(\partial\phi'/\partial\lambda)_{y=0,h} = 0$, which means that surface potential keeps constant while discharging (the CP boundary), we get

$$F_h = -k_bT\int_0^h\left(\sum_i n_i - \sum_i n_i^\infty\right)\mathrm{d}y - \frac{\varepsilon_0\varepsilon_r}{2}\int_0^h\left(\frac{\mathrm{d}\phi}{\mathrm{d}y}\right)^2\mathrm{d}y \quad \text{(constant potential)}, \tag{72}$$

and then EDL interaction energy can be calculated by Eq. (51). Verwey and Overbeek [76] recommended this method to calculate EDL interaction energy because its numerical integration is the easiest compared with other methods. However, today, about 70 years later with the popularization of computers, the advantage of this method is not that obvious. Plus, the CC or CR boundaries seem to be hard to be applied in this method.

4.1.3. Pressure integrating method

In this method, the disjoining pressure generated by EDL interaction, Π_{EDL}, is derived from thermodynamic equations, and then integrated to get the interaction energy. According to the Gibbs-Duham equation,

$$-S\mathrm{d}T + V\mathrm{d}p - \sum_i N_i \mathrm{d}\mu_i = 0 \tag{73}$$

Assume constant temperature and substitute $\mu_i = \mu_i^0 + k_bT\ln c_i + z_i e\phi$ into the above equation, then

$$\mathrm{d}p = \sum_i z_i e n_i \mathrm{d}\phi + k_bT\mathrm{d}\sum_i n_i, \tag{74}$$

Combined with the PB equation, the integration of Eq. (74) is [56].

$$p_y(h) - p_y(\infty) = -\frac{\varepsilon_0\varepsilon_r}{2}\left(\left(\frac{\mathrm{d}\phi}{\mathrm{d}y}\right)^2_{y(h)} - \left(\frac{\mathrm{d}\phi}{\mathrm{d}y}\right)^2_{y(\infty)}\right) + k_bT\left[\sum n_{i,y(h)} - \sum n_{i,y(\infty)}\right]. \tag{75}$$

It is easy to prove that $dp/dy = 0$. With the neglect of the Stern layer, Π_{EDL} can be calculated by the charging quantities on the first interface,

$$\begin{aligned}\Pi_{EDL}(h) &= p_{y=0}(h) - p_{y=0}(\infty)\\ &= -\frac{\sigma_{d1}^2(h) - \sigma_{d1}^2(\infty)}{2\varepsilon_0\varepsilon_r} + k_bT\Big[\sum n_i^\infty(\exp(-z_i\psi_{d1}(h))\\ &\quad - \exp(-z_i\psi_{d1}(\infty)))\Big],\end{aligned} \tag{76}$$

which is a general expression, and can be used with the CR boundary. Similarly, the other interface can also be used to calculate Π_{EDL}. If the CC boundary is assumed, then

$$\Pi_{EDL}(h) = k_bT\sum_i\Big(n_i^{S1}(h) - n_i^{S1}(\infty)\Big) \quad \text{(constant charge)}, \tag{77}$$

where n_i^{S1} is the ion number density on the 1st interface. So Eq. (77) is also called contact value theorem [56]. On the other hand, if the CP boundary is assumed, then

$$\Pi_{EDL}(h) = -\Big(\sigma_{d1}^2(h) - \sigma_{d1}^2(\infty)\Big)\Big/2\varepsilon_0\varepsilon_r \quad \text{(constant potential)}. \tag{78}$$

Then EDL interaction energy can be obtained by Eq. (52).

Now we will introduce some other forms of Π_{EDL} and w_{EDL} for specific systems. For symmetrical interfaces, $(d\phi/dy)_{y=h/2} = 0$, and the expression of Π_{EDL} (Eq. (76)) can be simplified as

$$\begin{aligned}\Pi_{EDL}(h) &= p_{y=h/2}(h) - p_{y=h/2}(\infty)\\ &= k_bT\sum(n_i^m - n_i^\infty) \quad (\psi_{d1} = \psi_{d2} = \psi_d),\end{aligned} \tag{79}$$

where $n_i^m = n_i^\infty\exp(-z_i\psi_m)$ is the ion number density at the middle plane. Further, for 1:1 electrolyte, when $\psi_m < 1$, $\sinh\psi_m \approx \psi_m$. Then Eq. (79) can be simplified as

$$\Pi_{EDL}(h) = k_bTn^\infty\psi_m^2 \quad (\zeta_1 = \zeta_2,\ \ \psi_m < 1,\ \ 1:1\ \text{electrolyte}). \tag{80}$$

Next, we can introduce the important linear superposition approximation (LSA). This approximation means that ψ_m is simply the sum of the potential at the mid plane generated by each interface, which is valid when the two EDLs are weakly overlapped. With this assumption, we can derive ψ_m from Eq. (7):

$$\psi_m = 4\ln\frac{1 + \tanh(\psi_d/4)\exp(-\kappa h/2)}{1 - \tanh(\psi_d/4)\exp(-\kappa h/2)}. \tag{81}$$

If $\psi_m < 1$, from Eq. (81) we know $\tanh(\psi_d/4)\exp(-\kappa h/2) < 0.125$. Thus Eq. (81) can approximately change to

$$\psi_m = 8\tanh(\psi_d/4)\exp(-\kappa h/2). \tag{82}$$

Substitute Eq. (82) into Eq. (80) and then integrate Eq. (80), we get [56]:

$$w_{EDL} = 64k_bTn^\infty\tanh^2(\psi_d/4)\exp(-\kappa h)\Big/\kappa \quad \text{(LSA solution)}, \tag{83}$$

Note that this equation also uses CP boundary, since ψ_d is assumed independent on h. For simplicity, in the following we refer to Eq. (83) as the LSA solution.

4.1.4. Summary

In the previous part of this section, we introduce three methods to derive EDL interaction energy, including surface charging method, electrolyte discharging method, and pressure integrating method. And we present solutions of EDL interaction under three kinds of boundary conditions, including constant potential (CP), constant charge (CC), and charge regulation (CR). These boundary conditions can largely affect the results; and the three methods lead to identical results with the same boundary conditions and other assumptions, as proved in Sec. 4.2.1.

We name the solutions of EDL interaction with non-simplified PB equation with different boundaries as accurate constant potential (ACP) solution, accurate constant charge (ACC) solution, and charge regulation (CR) solution. The three methods totally provide three ACP solutions (Eq. (65), Eq. (72), and Eq. (78)), two ACC solutions (Eq. (63) and Eq. (77)), and two CR solutions (Eq.(61)-(62) and Eq. (76)). Except that the electrolyte discharging method only provide a ACR solution (Eq. (72)), the other two methods respectively provide one ACP, one ACC, and one CR solution.

We also introduce two solutions of EDL interaction with simplifications for the PB equation, including the HHF equation (Eq. (66)) and the LSA solution (Eq. (83)). Both of them assume the CP boundary and are very convenient to use. HHF equation uses Debye-Hückel linear approximation; while the LSA solution is derived under linear superposition approximation. Therefore, compared with the HHF equation, the LSA solution can be used for high zeta potential interfaces, but is quickly invalid if two EDLs are strongly overlapped. In addition, the HHF equation can describe the dissimilar interfaces while LSA solution cannot. The approximate solutions of EDL interaction energy with the CC boundary are not as simple as the HHF equation and the LSA solution [56], and are not discussed in this paper.

4.2. Discussion

4.2.1. The unity of the three methods

The three methods produce equivalent expressions for EDL interaction with the same boundaries. In another word, the ACC solutions (Eq. (63) and Eq. (77)) are equivalent; the ACP solutions (Eq. (65), Eq. (72), and Eq. (78)) are equivalent; and the CR solutions (Eq.(61)-(62) and Eq. (76)) are equivalent. These equivalences can be easily proved by numerical computation; in this section, we will analytically prove the equivalence of ACP solutions for symmetrical interfaces with $\sigma_0 < 0$ [76]. We use I, II, III to differentiate the ACP solutions by the three methods, in the order they appear in Sec. 4.1.

First, we can rewrite Eq. (72) as

$$\begin{aligned}F_h[\text{II}] &= -k_bT\int_0^h\Big(\sum_i n_i - \sum_i n_i^m + \sum_i n_i^m - \sum_i n_i^\infty\Big)dy\\ &\quad - \frac{\varepsilon_0\varepsilon_r}{2}\int_0^h(d\phi/dy)^2dy\\ &= -\varepsilon_0\varepsilon_r\int_0^h(d\phi/dy)^2dy - k_bT\Big(\sum_i n_i^m - \sum_i n_i^\infty\Big)h\\ &= -2\sqrt{2k_bT\varepsilon_0\varepsilon_r}\int_{\phi_0}^{\phi_m}\sqrt{\sum_i n_i - \sum_i n_i^m}\,d\phi - k_bT\Big(\sum_i n_i^m\\ &\quad - \sum_i n_i^\infty\Big)h.\end{aligned} \tag{84}$$

Therefore,

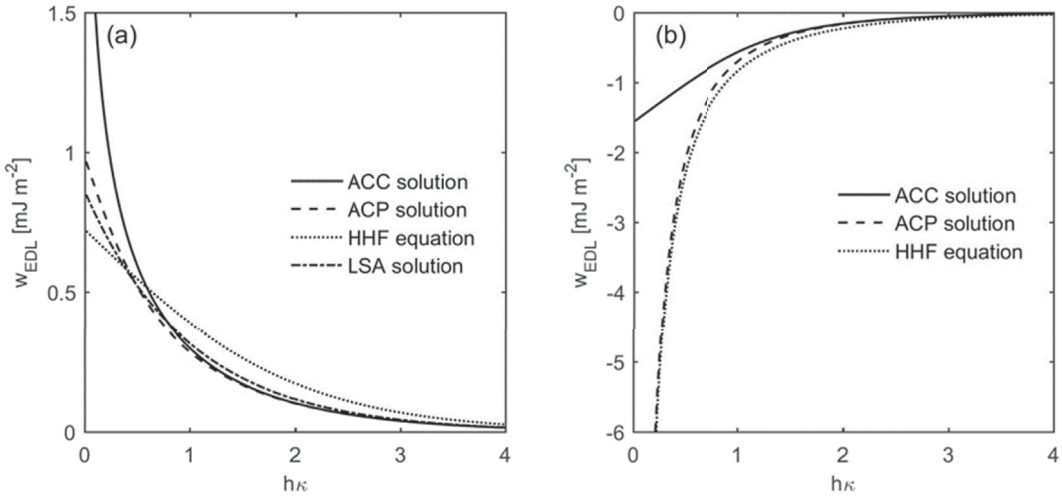

Fig. 9. The EDL interaction energy along with the dimensionless water film thickness $h\kappa$ at 298 K for (a) $\zeta_1(h=\infty)=\zeta_2(h=\infty)=-0.1$ V and (b) $-\zeta_1(h=\infty)=\zeta_2(h=\infty)=-0.1$ V. The electrolyte is 1:1 with bulk concentration 0.001 M.

$$\begin{aligned}\Pi_{EDL}[\mathrm{II}] &= -\frac{\mathrm{d}F_h}{\mathrm{d}h}\\ &= -2\sqrt{2k_bT\varepsilon_0\varepsilon_r}\int_{\phi_0}^{\phi_m}\frac{1}{2}\Big(\sum_i n_i-\sum_i n_i^m\Big)^{-1/2}\frac{\mathrm{d}}{\mathrm{d}h}\sum_i n_i^m\mathrm{d}\phi\\ &\quad -2\sqrt{2k_bT\varepsilon_0\varepsilon_r}\,\frac{\mathrm{d}\phi_m}{\mathrm{d}h}\sqrt{\sum_i n_i^m-\sum_i n_i^m}\\ &\quad +k_bTh\frac{\mathrm{d}}{\mathrm{d}h}\sum_i n_i^m+k_bT\Big(\sum_i n_i^m-\sum_i n_i^\infty\Big)\\ &= -2k_bT\frac{\mathrm{d}}{\mathrm{d}h}\sum_i n_i^m\int_{\phi_0}^{\phi_m}(\mathrm{d}\phi/\mathrm{d}y)^{-1}\mathrm{d}\phi+k_bTh\frac{\mathrm{d}}{\mathrm{d}h}\sum_i n_i^m\\ &\quad +k_bT\Big(\sum_i n_i^m-\sum_i n_i^\infty\Big)\\ &= k_bT\Big(\sum_i n_i^m-\sum_i n_i^\infty\Big),\end{aligned}\tag{85}$$

which is equivalent to Eq. (78) for symmetrical interfaces. To prove the identity between method 1 and method II, we aim to prove that at a certain h,

$$\frac{\partial F_h[\mathrm{I}]}{\partial\phi_0}=\frac{\partial F_h[\mathrm{II}]}{\partial\phi_0}\tag{86}$$

Since when $\phi_0=0$, both $F_h[\mathrm{I}]$ and $F_h[\mathrm{II}]$ are zero, so Eq(86) is identical to $F_h[\mathrm{I}]=F_h[\mathrm{II}]$. From Eq. (65),

$$\frac{\partial F_h[\mathrm{I}]}{\partial\phi_0}=-2\sigma_0,\tag{87}$$

while from Eq. (84),

$$\begin{aligned}\frac{\partial F_h[\mathrm{II}]}{\partial\phi_0} &= -2\sqrt{2k_bT\varepsilon_0\varepsilon_r}\left(\int_{\phi_0}^{\phi_m}-\frac{1}{2}\Big(\sum_i n_i-\sum_i n_i^m\Big)^{-1/2}\frac{\partial}{\partial\phi_0}\sum_i n_i^m\mathrm{d}\phi\right.\\ &\quad\left.-\sqrt{\sum_i n_i^S-\sum_i n_i^m}\right)-k_bT\frac{\partial}{\partial\phi_0}\sum_i n_i^m h\\ &= 2\sqrt{2k_bT\varepsilon_0\varepsilon_r\Big(\sum_i n_i^S-\sum_i n_i^m\Big)}=-2\sigma_0.\end{aligned}\tag{88}$$

Therefore, Eq. (86) is valid. So far we have proved the identity of the three methods under constant potential assumption for symmetrical interfaces.

4.2.2. Convergence analysis

In the following, we will discuss the convergence of the solutions of EDL interaction with CP, CC, and CR boundaries as $h\to 0$, using the expressions provided by the pressure integrating method. The following analysis is based on the convergence analysis of interface charging quantities in Sec. 3.5.

For the CC boundary, based on Eq. (48) and Eq. (77), we can know that

$$h\to 0:\quad \Pi_{EDL}(h)\to\begin{cases}-k_bT(\sigma_{d1}+\sigma_{d2})\big(hez^*\big)^{-1}, & \text{if } \sigma_{d1}+\sigma_{d2}\neq 0\\ k_bT\sum_i n_i^\infty\big(1-\exp(-z_ie\zeta(\infty)/k_bT)\big), & \text{if } \sigma_{d1}+\sigma_{d2}=0\end{cases}\quad(\text{constant charge}).\tag{89}$$

where $z^* = (\sigma_{d1} + \sigma_{d2})^{-1}\min_i((\sigma_{d1} + \sigma_{d2})z_i)$. Therefore, if $\sigma_{d1} + \sigma_{d2} = 0$, Π_{EDL} becomes a constant when $h \to 0$, otherwise $\Pi_{EDL} \to +\infty$. This can lead to an unphysical repulsion between two oppositely charged interfaces. Further we can indicate that w_{EDL} behaves similarly based on Eq. (52). The analysis is consistent with the numerical ACC solution, as shown in Fig. 9.

For the CP boundary, based on Eq. (49) and Eq. (78), we can know that

$$h \to 0: \quad \Pi_{EDL}(h) \to -\frac{\varepsilon_0 \varepsilon_r}{2}\left(\frac{(\zeta_1 - \zeta_2)^2}{h^2} - \sigma_{1d}^2(\infty)\right) \quad \text{(constant potential)}. \tag{90}$$

Therefore, if $\zeta_1 = \zeta_2$, Π_{EDL} becomes a constant when $h \to 0$, otherwise $\Pi_{EDL} \to -\infty$. This can lead to an unphysical attraction between two similarly charged interfaces. Further we can indicate that w_{EDL} behaves similarly based on Eq. (52). The HHF equation and LSA solution both assume CP boundary, so they have the same tendencies. The analysis is consistent with the numerical ACP solution, HHF equation, and LSA solution, as shown in Fig. 9.

For the CR boundary, we can also discuss the convergence of Π_{EDL} when $h \to 0$ based on Sec. 3.5 and Eq. (76). If $\alpha_1 + \alpha_2 < 0$ and $\beta_1 + \beta_2 > 0$, Π_{EDL} is always finite; if $\alpha_1 = \alpha_2 = 0$ and $\beta_1 + \beta_2 > 0$, or $\alpha_1 + \alpha_2 < 0$ and $\beta_1 = \beta_2 = 0$, $\Pi_{EDL} \to +\infty$; and if $\alpha_1 = \alpha_2 = 0$ and $\beta_1 = \beta_2 = 0$, $\Pi_{EDL} = 0$. Therefore, the CR boundary does not lead to the unphysical infinite attraction. Besides, the infinite repulsion is produced for interfaces that can only be similarly charged, thus the sign for EDL interaction is physical; and the value is less extreme than that for the CC boundary since ζ_1 and ζ_2 are less extreme. In addition, we can infer that, for two different and not totally reversal interfaces, the ACC solution always overestimates the Π_{EDL} compared with CR solution as $h \to 0$, and the ACP solution always underestimates that. In Sec. 4.3, we will take the oil N/P-NaCl(aq) -silica systems as two examples to analyze.

4.3. Case analysis: polar oil-NaCl (aq)-silica system

In this section, we take oil N/P-NaCl (aq)-silica systems with bulk concentration $c = 0.001$ M, $T = 298$ K, pH = 7 as two examples to calculate the EDL interaction, one of which should behave repulsive while the other attractive. The charging models as described in Sec. 3.6 are used for the charge CR solution. Since these two interfaces bear unequal charges, actually LSA solution cannot be directly used; here we use the mean of the two zeta potentials when $h \to \infty$ to calculate LSA solution for similarly charged interfaces. We can have the following discussions based on the results shown in Fig. 10.

(1) When $h > 2/\kappa$, the CR, ACC, ACP, LSA solutions lead to similar results. This is because the EDLs are weakly overlapped, and charge regulation is still not significant (as shown in Figs. 7 and 8). The HHF deviates from other solutions, because $|\zeta_1|, |\zeta_2| > 25$ mV and the Debye-Hückel assumption fails down for the two studied cases.
(2) When $h < 2/\kappa$, compared with the CR solution, the ACP solution underestimates EDL interaction, while the ACC solution overestimates that. This is due to the misestimation of the charging quantities, as discussed in Sec. 3.5.
(3) When $h < 0.2/\kappa$, only the CR solution leads to correct sign of EDL interaction energy for both systems. The ACC solution leads to unphysical repulsion for the oil P-NaCl (aq)-silica system, as also indicated by Eq. (89). The ACP solution and the HHF equation lead to unphysical attraction for oil N-NaCl (aq)-silica system, as also indicated by Eq. (90). Since the distance between charged interfaces near contact line may be smaller than 1 nm in wettability problems (as discussed in Sec. 5), it is safest to use the CR solution of EDL interaction energy to analyze ion-tuned wettability, to avoid unphysical interactions for various systems.
(4) The ACP solution behaves even worse than the LSA solution, because we simply assume identical interfaces to use the LSA solution but still dissimilar interfaces to calculate the ACP solution. This provides an idea to avoid the unphysical attraction due to the CP boundary: we can assume identical interfaces if the two interfaces are similarly charged. Similarly, we can assume totally reversal interfaces if the two interfaces are oppositely charged, to avoid the unphysical repulsion due to the CC boundary.

5. Wettability alteration by EDL interaction

This section introduces how to quantitatively determine the

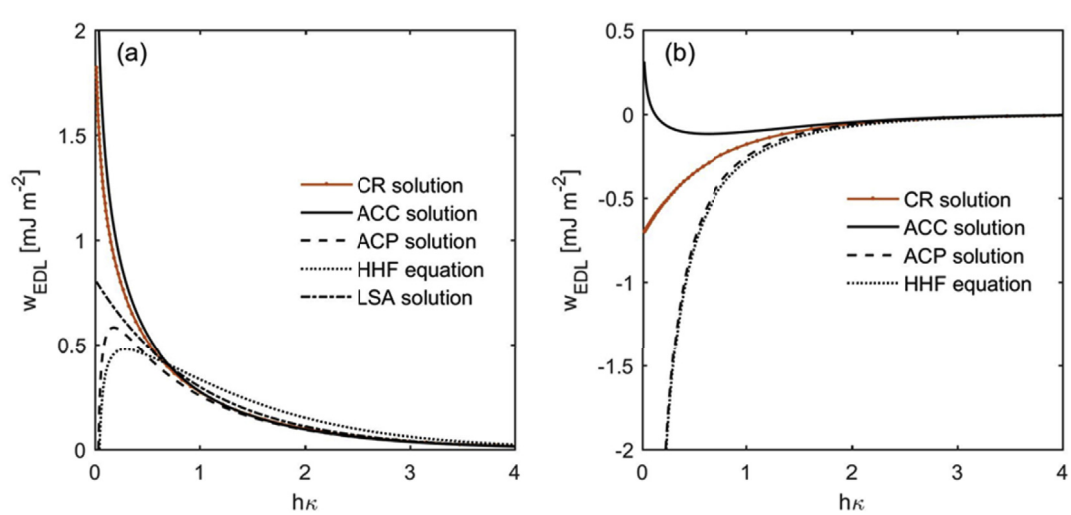

Fig. 10. The EDL interaction energy in (a) the oil N-NaCl (aq)- silica system and (b) the oil P-NaCl (aq)-silica system along with the dimensionless water film thickness $h\kappa$ at 298 K. The NaCl bulk concentration is 0.001 M, and the pH is 7.

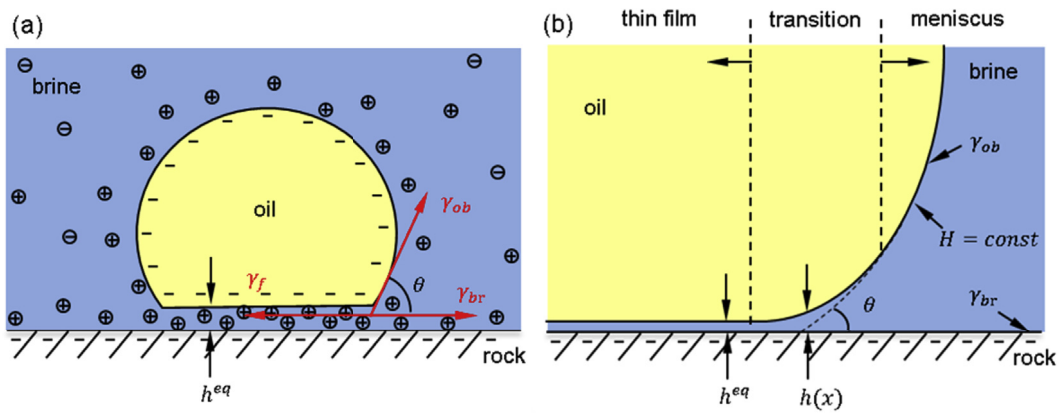

Fig. 11. (a) Macroscopic and (b) microscopic methods to derive the Young-Dupré equation.

contribution of EDL interaction to ion-tuned wettability. The water-phase contact angle θ is used to measure wettability, while the Darcy-scale wettability is not considered. The model system we analyze is shown in Fig. 11. First, in Sec.5.1, the Young-Dupré equation is introduced, which connects the contact angle with the equilibrium interaction energy between oil and rock. In Sec.5.2, the extended DLVO theory is introduced, and one simple relation between contact angle and EDL interaction energy is given. Finally, two typical OBR systems, whose charging quantities and typical EDL interaction curves have also been analyzed in Sec. 3.6 and 4.3, will be exemplified to analyze the contribution of EDL interaction to ion-tuned wettability in Sec. 5.3.

5.1. Young-Dupré equation

To derive the Young-Dupré equation, first some assumptions must be clarified. The rock surface is assumed to be solidified, planar, and smooth, so the effects of morphology and fines release that occur in the real OBR system are not considered. The system is supposed water-wet ($0^\circ \le \theta < 90^\circ$), to enable the existence of water film between oil and rock. The water film is thick (~10–100 nm) for $\theta \approx 0^\circ$ (totally water-wet), and is thin (~0.1–1 nm) for $0^\circ < \theta < 90^\circ$. For oil-wet systems, an oil film may form between brine and rock [56]. In this case, EDL interaction does not necessarily eliminate, and may also occur between the two oil-brine interfaces near contact line. But in the following analysis, we just consider the water-wet systems to avoid complex discussions.

The Young-Dupré equation can be derived from a macroscopic view (Fig. 11 (a)) or a microscopic view (Fig. 11 (b)) [46,93,94]. We will introduce the macroscopic view first. According to the Young equation,

$$\gamma_f = \gamma_{ob} \cos\theta + \gamma_{br}, \tag{91}$$

where γ_{ob} and γ_{br} are the interface tension of the oil-brine interface and brine-rock interface, and γ_f is expressed by the Dupré equation,

$$\gamma_f = \gamma_{ob} + \gamma_{br} + w^{eq}, \tag{92}$$

where w^{eq} is the equilibrium interaction energy per unit area between oil and solid in brine. The combination of Eq. (91) and Eq. (92) leads to the Young-Dupré equation

$$\theta = cos^{-1}(1 + w^{eq}/\gamma_{ob}). \tag{93}$$

In the microscopic view, very near the contact line, the shape of the interface is influenced by the surface forces, which zone is named as the transition zone, as shown in Fig. 11 (b). The dependence of interface shape on surface forces can be described by the augmented Young-Laplace equation [93].

$$H(h) = (P_c - \Pi(h))/2\gamma_{ob}, \tag{94}$$

where H is the curvature of the oil-brine interface, P_c the capillary pressure, and Π the disjoining pressure between oil and rock. Π is related to w^{eq} by

$$w^{eq} = \int_{h^{eq}}^{\infty} (\Pi(h) - P_c)\mathrm{d}h. \tag{95}$$

On the other hand, the transition zone is usually down to nanoscale and much smaller than the drop size, thus H can be expressed as

$$H(h(x)) \approx \left(1 + h'(x)^2\right)^{-1/3} |h''(x)|/2. \tag{96}$$

In the microscopic view, the contact angle is defined as the angle between the circle fitting the macroscopic interface and the rock surface. Combining Eq. (94)-(96), we can also derive Eq. (93) [93]. This derivation indicates that the surface forces act in the transition zone to influence wettability.

5.2. Extended DLVO theory

In this part, we will introduce the extended DLVO theory which describes the dependence of contact angle on EDL interaction and other colloidal forces. According to Eq. (93), contact angle is determined by the equilibrium interaction energy w^{eq} and the oil-brine interface tension γ_{ob}. γ_{ob} can be obtained easily from experiments. In order to find w^{eq}, the variation of interaction energy w along with the water film thickness h must be clear. We know that

$$w = \int_{h}^{\infty} (\Pi(h) - P_c)\mathrm{d}h, \tag{97}$$

and Π can be expressed as

$$\Pi = \Pi_{str} + \Pi_{EDL} + \Pi_{ad}, \tag{98}$$

where Π_{str} is the structural repulsive force, Π_{EDL} is the force

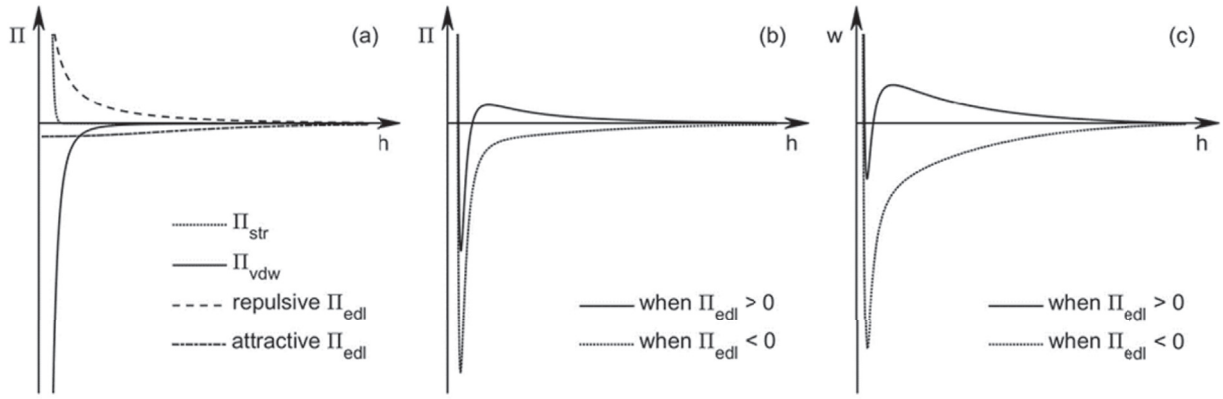

Fig. 12. Schemes for (a) component disjoining pressure, (b) total disjoining pressure, and (c) total interaction energy along with the water film thickness.

induced by EDL interaction which can be attractive or repulsive, and Π_{ad} includes all the other attractive forces such as van der Waals force, cation bridging and so on. Structural force rises very steeply to infinity when h gets smaller than a critical value, while usually EDL interaction has the longest operating range among the three kinds of forces, as shown in Fig. 12(a). For a macroscopic drop with radius much larger than EDL thickness, the H in the transition zone is much larger than the macroscopic drop curvature, and thus $P_c \ll |\Pi|$ and the P_c in Eq. (97) may be neglected. Then w can also be separated as:

$$w = w_{str} + w_{EDL} + w_{ad}. \tag{99}$$

Two examples of disjoining pressure and interaction energy along with water film thickness are shown in Fig. 12 (b) (c), in one of which EDL interaction behaves strongly repulsive and in the other attractive. More cases can be found in Refs. [46,76]. If the EDL interaction behaves strongly repulsive, an energy barrier (a local maximum point) can form. When an oil drop approaches to the rock pre-wet by brine, the energy barrier can prevent oil to go closer to rock, to generate a thick water film. If the energy barrier is overcome by external fluctuations or forces, the thick water film breaks down and w^{eq} becomes the minimum value on the curve. When the rock is pre-wet by oil, the energy barrier helps the energy be trapped at the minimum point. If EDL interaction behaves attractive, no energy barrier can form, and the minimum interaction energy is always negative. In the following, the water film is assumed thin and contact angle is evaluated at the minimum point of the energy curve. If the minimum energy is positive, the OBR system is totally water-wet; otherwise the system has a finite contact angle.

h^{eq} is approximately only determined by the structural force if Π_{str} is extremely strong and decays very quickly. Meanwhile w_{str}^{eq} can be very small since the distance for force integration is nearly zero. Therefore, the effect of structural force on w^{eq} is only reflected on the value of h^{eq}, and

$$w^{eq} \approx w_{EDL}^{eq} + w_{ad}^{eq}. \tag{100}$$

Under the assumption that w_{ad} and h^{eq} do not change with ionic composition, the variation of w^{eq} is mainly determined by EDL interaction. We define the initial contact angle unaffected by EDL as $\theta_0 = \cos^{-1}(1 + w_{ad}^{eq}/\gamma_{ob})$, then rewrite Eq. (93) as

$$\theta = cos^{-1}(\cos\theta_0 + w_{EDL}^{eq}/\gamma_{ob}), \tag{101}$$

which clearly presents the contribution of EDL interaction to ion-tuned contact angle.

Since the distance between oil and rock in the transition zone is

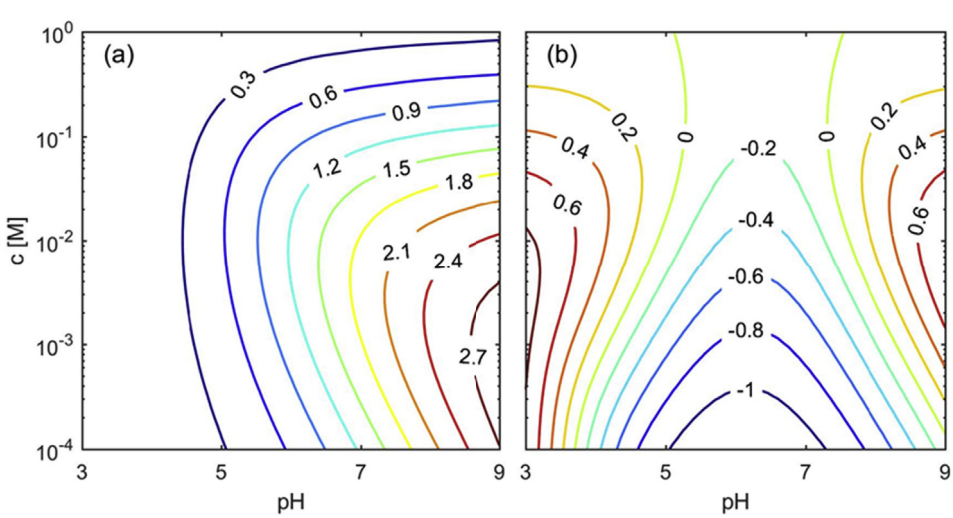

Fig. 13. The charge regulation (CR) solution of EDL interaction energy (unit: mN m^{-1}) in (a) the oil N-NaCl (aq)-silica system and (b) the oil P- NaCl (aq) -silica system for different ionic composition at 298 K.

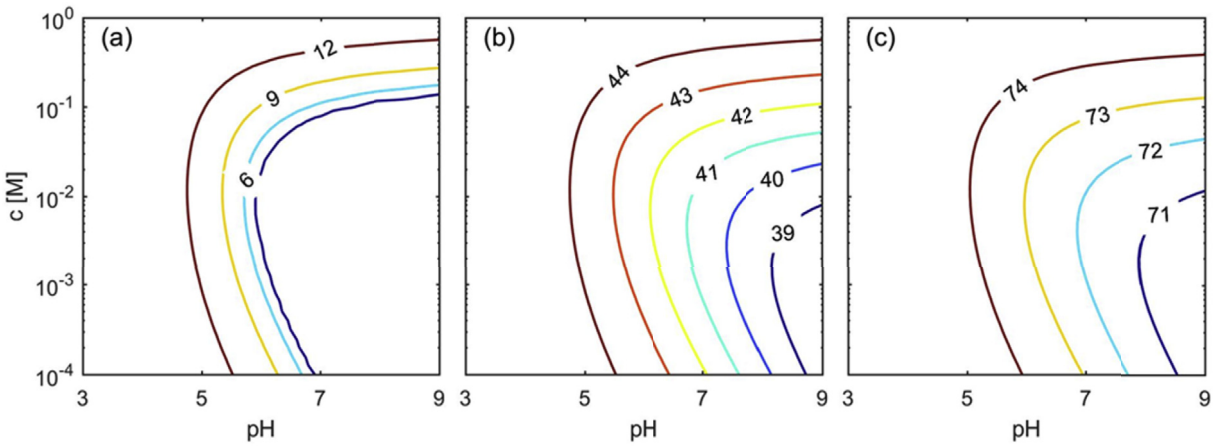

Fig. 14. The contact angle (unit: degree) of the oil N-NaCl (aq)-silica system for different ionic composition at 298 K, for three initial wettability (a) $\theta_0 = 15°$, (b) $\theta_0 = 45°$ and (c) $\theta_0 = 75°$.

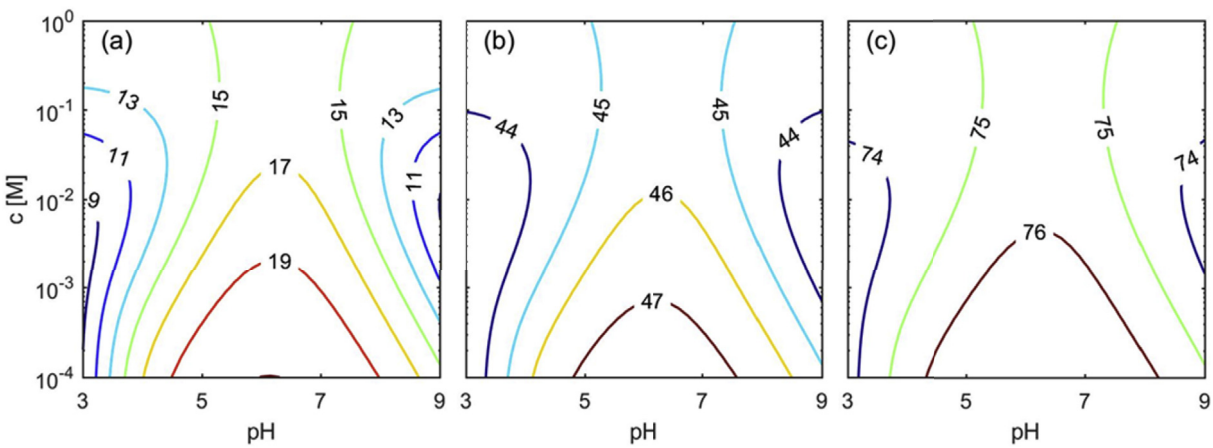

Fig. 15. The contact angle (unit: degree) of the oil P-NaCl (aq)-silica system for different ionic composition at 298 K, for three initial wettability (a) $\theta_0 = 15°$, (b) $\theta_0 = 45°$ and (c) $\theta_0 = 75°$.

down to nanometers, the interface potential and charge density must be dependent on location due to EDL interaction. Therefore, it is better to use charge regulation solutions of EDL interaction, as discussed in Sec.4.2.2. and Sec.4.3.

5.3. Case analysis: polar oil-NaCl (aq) -silica system

In this section, we present the contact angle variation due to EDL interaction, using Eq. (101) and the charge regulation (CR) solution of EDL interaction energy. We choose the CR solution for the reasons discussed in Sec. 4.2.2. and Sec. 4.3. Two systems are considered: oil P-NaCl (aq)-silica system and oil N-NaCl (aq)-silica system, whose charging quantities for single EDL, charge regulation for two interacting EDLs, and typical EDL interaction curves have been presented in Sec. 3.6 and Sec. 4.3. The constants for contact angle analysis are $\gamma_{ob} = 36$ mN m^{-1}, and $h^{eq} = 0.16$ nm. The temperature is 298 K. The interaction energy w_{ad}^{eq} is assumed independent on ionic composition, and is given artificially by setting different initial contact angles θ_0. Note that h^{eq} may have an important effect on the results, but its determination may be difficult considering the hydration force is hard to be accurately described by the classical theory. Here we take $h^{eq} = 0.16$ nm (near to 0.158 nm suggested by Ref. [94]), note that it may be unrealistic and just is taken as a calculation parameter.

EDL interaction energy at h^{eq} for different pH and concentration of the oil P/N-NaCl (aq)-silica system is shown in Fig. 13. Then the contour maps for contact angle are respectively shown in Figs. 14 and 15. Based on the results, we can have the following discussions.

(1) The contact angle maps shown in Figs. 14 and 15 indicate that the contact angle variation due to EDL interaction is less than 20°. This is somehow not quite significant.
(2) For the oil N-NaCl (aq) -silica system, the EDL interaction always behaves repulsive, and makes the system more water-wet, as shown in Figs. 13(a) and 14. The EDL repulsion always enhances with the increase of pH, but has a non-monotonic relation with concentration. For 0.01 M $< c <$ 1 M, the decrease of concentration may enhance EDL repulsion. For 0.0001 M $< c <$ 0.01 M, the concentration effect is weak and even a little reversal. This non-monotonicity can be explained as below. EDL repulsion is determined by the variation of zeta potential and surface charge density with water film thickness. At very low concentration, though the variation of zeta potential is large, the variation of surface charge density is restricted. In this case, the increase of pH may significantly enhance EDL repulsion.
(3) For the oil P-NaCl (aq)-silica system, the EDL interaction behaves repulsive and make the system more water-wet at very high or low pH, while behaves attractive and make the

system more oil-wet at middle pH, as shown in Figs. 13(b) and 15. At very high pH, the oil charge is nearly neutral while the silica is very negatively charged; and at very low pH, the oil is very positively charged while the silica is nearly neutral. Since the EDL interaction between one uncharged interface and one charged interface is always repulsive, as can be indicated by Sec. 4, the EDL interaction behaves repulsive at very high or very low pH. At medium pH, the oil and the silica are almost reversely charged, so the EDL interaction behaves attractive; and the decrease of concentration enhances the EDL attraction and makes the OBR system more oil-wet, as experimentally proved by Ref. [67].

(4) Figs. 14 and 15 also present the effect of initial wettability on ion-tuned wettability induced by EDL interaction. For very water-wet cases, the contact angle variation may be restricted because the contact angle cannot be smaller than zero, and for near neutral wet cases, the contact angle variation is also restricted because the attractive force is too large. Besides, for very strongly water-wet cases oil drop can be trapped in pores of rock. Therefore, if EDL repulsion is the main mechanism for ion-tuned wettability in sandstone during LSF, we can infer that the benefit brought by LSE compared with regular waterflooding is most significant for middle water-wet cases, which phenomenon has been experimentally proved by Ref. [95].

6. Discussion and perspectives

6.1. Boundary conditions of two interacting EDLs

By reviewing the theories of EDL interaction and contact angle, and analyzing the convergence of charging quantities and EDL interaction energy at small water film thickness, we suggest that the boundary conditions should be carefully treated to study the contribution of EDL interaction to contact angle. The reason is that the water film chould be very thin to produce a finite contact angle in an OBR system. To integrate the EDL interaction energy, the variation of charging quantities with water film thickness should be well described, and the commonly used constant potential (CP) boundary or constant charge (CC) boundary may lead to great errors for thin water films. Unless the charges of the two interfaces are nearly identical, the CP boundary will lead to infinite surface charge densities, and even lead to unphysical EDL attraction between two similarly charged interfaces. On the other hand, unless the charges of the two interfaces are nearly reversal, the CC boundary will lead to infinite zeta potential, and may even produce unphysical EDL repulsion between two oppositely charged interfaces. In comparison, charge regulation (CR) boundary always lead to physical sign and less extreme EDL interaction, thus is safer to be used.

Under some circumstances, there is a simple way to avoid the unphysical sign of EDL interaction without using the complex CR boundary. If two interfaces are similarly charged, and ζ_1 does not differ too much from ζ_2, we can safely use the CP boundary by assuming that the two interfaces are identical with zeta potential as $(\zeta_1 + \zeta_2)/2$. If the two interfaces are oppositely charged, and σ_{d1} is close to $-\sigma_{d2}$, we can safely use the CC boundary by assuming that the two interfaces are reversal to each other with absolute surface charging density as $(|\sigma_{d1}| + |\sigma_{d2}|)/2$. Of course, in this way the magnitude of EDL interaction energy still deviates from that in the CR solution.

6.2. Understanding of ion-tuned wettability

This part discusses how this review helps us understand more about ion-tuned wettability. First, we clarify the facts indicated by the EDL theory but may be constantly neglected. The EDL interaction is not purely dependent on zeta potential; it is also related to the variation of surface charge density along with the water film thickness. Since very dilute solutions cannot provide much variation of surface charging density when oil and rock are similarly charged, EDL repulsion can be slightly weakened at extremely low concentration. In contrast, when oil and rock are oppositely charged, lower concentration always enhances EDL attraction and makes the system more oil-wet. In addition, for middle water-wet cases, the EDL interaction can contribute most to ion-tuned wettability.

In real OBR systems, the contact angle variation according to the theoretical analysis is usually slightly smaller than the experimental observations on mica surfaces [59,60] or carbonate surfaces [42], and much smaller than those given by Ref. [61] on clay surface. We infer that the morphology of the real rock surface is probable to enhance the wettability alteration by EDL interaction. Rock surfaces, especially clay, have many sub-structures. Some surface parts are oil-wet due to oil-aging, while some inner parts are water-wet due to brine-saturating, as shown in Fig. 2. If the clay-clay cohesion is not strong and can be overcome by EDL repulsion among clays, then fines migration may be induced to make the system more water-wet, as shown in Fig. 2(a) and discussed in detail in Sec. 2.2. If the clay-clay cohesion is very strong and not easy to be broken, then EDL interaction between oil and rock just need to break several pins connecting oil and rock to alter wettability, as shown in Fig. 2(b). The above two conditions can both make the experimentally observed ion-tuned wettability more significant than that predicted by theory.

We can also have some speculations for the acting of hydration force and MIE by comparing with experiments. The EDL interaction at high concentration is usually very limited according the analysis before. According to previous experiments, at extremely high salinity, experiments usually show more water-wet conditions with 1:1 electrolyte while usually show more oil-wet conditions with multicomponent brine. We infer that at high concentration, hydration force and ion binding dominate OBR interactions. For a 1:1 electrolyte, ion binding is rare or weak, and only hydration force dominates to make the system more water-wet; while for multicomponent brine, the hydration force competes with ion binding, and if ion binding wins the system can be more oil-wet.

In application, due to the reaction on rock surface, the water in sandstones during LSF is usually weakly alkaline, which enhances wettability alteration, and optimum salinity may be case by case. Extended to IDF both in sandstones and carbonates, we can conclude that when salinity is too low to show further LSE, adding potential determining ions may bring significant benefits. For example, weakly alkaline low salinity water may be used to enhance oil recovery in sandstones.

6.3. Current limitations and perspectives

Actually, the classical EDL model described in this review is simplified too much to analyze interfacial interaction in the transition zone. First, at high concentration (non-ideal solution), the Boltzmann distribution will fail and the finite volume of ions (steric effects) must be considered [96–98]. Second, polarization of solvent very near the interface may lead to large variation of dielectric constants [97–100]. Third, the oil-water interface should not be molecularly smooth, thus planar surface assumption may be problematic at small scales [101]. Fourth, there may exist ion exchange across the oil-water interface [101]. Though there exists an EDL theory to involve steric effects and solvent polarization [97,98], the coupling of these theories with surface charge model has not

been fully developed. Besides, the theory of EDL interaction energy also neglects or oversimplifies the contribution of Stern layer. In this paper, we just use a charge regulation model based on the classical EDL theory to provide a primary understanding of EDL interaction. Statistical thermodynamics or molecular simulation may be necessary to fully describe EDL interaction in the transition zone.

Besides, the effect of rock geometry on ion-tuned wettability by EDL interaction cannot be considered by the simple one-dimensional model in this work. Firstly, the model assumes flat rock surface and cannot include the inner morphology of rock, such as the porous structure of clay and matrix, which may enhance the wettability alteration by EDL interaction as discussed in Sec. 6.2. Secondly, the model in this work assumes infinitely large pore size and macroscopic drop. However, some rocks have many nanopores, where EDLs at pore surfaces can be overlapped; besides, oil confined in these pores may be in the form of nanodrops or nano-capillary columns, where macroscopic wetting theory introduced in Sec. 5 can be invalid. It will be interesting to use two- or three-dimensional simulations to explore whether these effects can bring much difference to ion-tuned wettability induced by EDL interaction.

Furthermore, some important physical or chemical processes are neglected in the current model. Firstly, the quantitative contribution of hydration force and MIE to ion-tuned wettability is still not effectively established, which requires some molecular-scale understanding of interfacial interaction. Secondly, some time-related pore-scale processes, such as non-equilibrium ionic diffusion, adsorption and multiphase flow, are to be considered to predict the typical time to allow wettability alteration. Finally, the upscaling of above molecular-scale and pore-scale processes is needed to direct field-scale production.

7. Conclusions

To conclude, this paper reviews the possible mechanisms of ion-tuned wettability, and proves the importance to understand the role of EDL interaction. A comprehensive theoretical framework to calculate the contribution of EDL interaction to ion-tuned wettability is given, and the boundary conditions of two interacting EDLs are emphasized in this issue. Based on the theories, two typical OBR systems are quantitatively analyzed to shed some light on the understanding of ion-tuned wettability. Further studies need be done to provide a three-dimensional, multi-process, multi-scale and time-related view of ion-tuned wettability.

Acknowledgements

This work is financially supported by the NSF grant of China (No. 91634107, 51676107), National Science and Technology Major Project on Oil and Gas (No. 2017ZX05013001).

References

[1] N.R. Morrow, Wettability and its effect on oil-recovery, J. Petrol. Technol. 42 (12) (1990) 1476–1484.
[2] G.Q. Tang, N.R. Morrow, Salinity, temperature, oil composition, and oil recovery by waterflooding, SPE Reservoir Eng. 12 (4) (1997) 269–276.
[3] N.R. Morrow, et al., Prospects of improved oil recovery related to wettability and brine composition, J. Petrol. Sci. Eng. 20 (3–4) (1998) 267–276.
[4] G.Q. Tang, N.R. Morrow, Influence of brine composition and fines migration on crude oil/brine/rock interactions and oil recovery, J. Petrol. Sci. Eng. 24 (2–4) (1999) 99–111.
[5] Y. Zhang, N.R. Morrow, Comparison of secondary and tertiary recovery with change in injection brine composition for crude-oil/sandstone combinations, in: SPE/DOE Symposium on Improved Oil Recovery, Society of Petroleum Engineers, 2006.
[6] Y. Zhang, X. Xie, N.R. Morrow, Waterflood performance by injection of brine with different salinity for reservoir cores, in: SPE Annual Technical Conference and Exhibition, Society of Petroleum Engineers, 2007.
[7] A. Lager, et al., Low salinity oil recovery - an experimental investigation, Petrophysics 49 (1) (2008) 28–35.
[8] H. Pu, et al., Low salinity waterflooding and mineral dissolution, in: SPE Annual Technical Conference and Exhibition, Society of Petroleum Engineers, 2010.
[9] S. Gamage, P. Hasanka, G.D. Thyne, Comparison of oil recovery by low salinity waterflooding in secondary and tertiary recovery modes, in: SPE Annual Technical Conference and Exhibition, Society of Petroleum Engineers, 2011.
[10] T. Hassenkam, et al., Pore scale observation of low salinity effects on outcrop and oil reservoir sandstone, Colloid. Surface. A Physicochem. Eng. Aspect. 390 (1) (2011) 179–188.
[11] T. Hassenkam, et al., The low salinity effect observed on sandstone model surfaces, Colloid. Surface. A Physicochem. Eng. Aspect. 403 (2012) 79–86.
[12] W. Winoto, et al., Secondary and tertiary recovery of crude oil from outcrop and reservoir rocks by low salinity waterflooding, in: SPE Improved Oil Recovery Symposium, Society of Petroleum Engineers, 2012.
[13] A.M. Shehata, H.A. Nasr-El-Din, Reservoir connate waterchemical composition variations effect on low-salinity waterflooding, in: Abu Dhabi International Petroleum Exhibition and Conference, Society of Petroleum Engineers, 2014.
[14] B. Suijkerbuijk, et al., Low salinity waterflooding at West Salym: laboratory experiments and field forecasts, in: SPE EOR Conference at Oil and Gas West Asia, Society of Petroleum Engineers, 2014.
[15] K.J. Webb, C.J.J. Black, H. Al-Ajeel, Low salinity oil recovery-log-inject-log, in: SPE/DOE Symposium on Improved Oil Recovery, Society of Petroleum Engineers, 2004.
[16] E.P. Robertson, Low-salinity waterflooding to improve oil recovery-historical field evidence, in: SPE Annual Technical Conference and Exhibition, Society of Petroleum Engineers, 2007.
[17] A. Lager, et al., LoSal enhanced oil recovery: evidence of enhanced oil recovery at the reservoir scale, in: SPE Symposium on Improved Oil Recovery, Society of Petroleum Engineers, 2008.
[18] J. Seccombe, et al., Demonstration of low-salinity EOR at interwell scale Endicott field Alaska, in: SPE Improved Oil Recovery Symposium, Society of Petroleum Engineers, 2010.
[19] H. Mahani, et al., Analysis of field responses to low-salinity waterflooding in secondary and tertiary mode in Syria, in: SPE EUROPEC/EAGE Annual Conference and Exhibition, Society of Petroleum Engineers, 2011.
[20] K. Skrettingland, et al., Snorre low-salinity-water injection–coreflooding experiments and single-well field pilot, SPE Reservoir Eval. Eng. 14 (02) (2011) 182–192.
[21] S. Law, P.G. Sutcliffe, S.A. Fellows, Secondary application of low salinity waterflooding to Forties sandstone reservoirs, in: SPE Annual Technical Conference and Exhibition, Society of Petroleum Engineers, 2014.
[22] G.R. Jerauld, et al., Modeling low-salinity waterflooding, SPE Reservoir Eval. Eng. 11 (06) (2008) 1,000–1,012.
[23] K.S. Sorbie, I. Collins, A proposed pore-scale mechanism for how low salinity waterflooding works, in: SPE Improved Oil Recovery Symposium, Society of Petroleum Engineers, 2010.
[24] P.V. Brady, J.L. Krumhansl, A surface complexation model of oil–brine–sandstone interfaces at 100°C: low salinity waterflooding, J. Petrol. Sci. Eng. 81 (2012) 171–176.
[25] C.T.Q. Dang, et al., Modeling low salinity waterflooding: ion exchange, geochemistry and wettability alteration, in: SPE Annual Technical Conference and Exhibition, Society of Petroleum Engineers, 2013.
[26] A. Kazemi Nia Korrani, G.R. Jerauld, K. Sepehrnoori, Coupled geochemical-based modeling of low salinity waterflooding, in: SPE Improved Oil Recovery Symposium, Society of Petroleum Engineers, 2014.
[27] A. RezaeiDoust, et al., Smart water as wettability modifier in carbonate and sandstone: a discussion of similarities/differences in the chemical mechanisms, Energy Fuel. 23 (9) (2009) 4479–4485.
[28] R.A. Nasralla, H.A. Nasr-El-Din, Impact of cation type and concentration in injected brine on oil recovery in sandstone reservoirs, J. Petrol. Sci. Eng. 122 (2014) 384–395.
[29] H.O. Yildiz, N.R. Morrow, Effect of brine composition on recovery of Moutray crude oil by waterflooding, J. Petrol. Sci. Eng. 14 (3–4) (1996) 159–168.
[30] T. Austad, et al., Seawater as IOR fluid in fractured chalk, in: SPE International Symposium on Oilfield Chemistry, Society of Petroleum Engineers, 2005.
[31] S. Strand, E.J. Høgnesen, T. Austad, Wettability alteration of carbonates—effects of potential determining ions (Ca2+ and SO42−) and temperature, Colloid. Surface. A Physicochem. Eng. Aspect. 275 (1–3) (2006) 1–10.
[32] P. Zhang, T. Austad, Wettability and oil recovery from carbonates: effects of temperature and potential determining ions, Colloid. Surface. A Physicochem. Eng. Aspect. 279 (1) (2006) 179–187.
[33] P. Zhang, M.T. Tweheyo, T. Austad, Wettability alteration and improved oil recovery by spontaneous imbibition of seawater into chalk: impact of the potential determining ions Ca 2+, Mg 2+, and SO 4 2−, Colloid. Surface. A Physicochem. Eng. Aspect. 301 (1) (2007) 199–208.
[34] A.A. Yousef, et al., Laboratory investigation of novel oil recovery method for carbonate reservoirs, in: Canadian Unconventional Resources and International Petroleum Conference, Society of Petroleum Engineers, 2010.
[35] T. Austad, et al., Conditions for a low-salinity enhanced oil recovery (EOR)

effect in carbonate oil reservoirs, Energy Fuel. 26 (1) (2011) 569–575.
[36] A. Al Harrasi, R.S. Al-maamari, S.K. Masalmeh, Laboratory investigation of low salinity waterflooding for carbonate reservoirs, in: Abu Dhabi International Petroleum Conference and Exhibition, Society of Petroleum Engineers, 2012.
[37] A. Al-adasani, B. Bai, Y.-S. Wu, Investigating low salinity waterflooding recovery mechanisms in carbonate reservoirs, in: SPE EOR Conference at Oil and Gas West Asia, Society of Petroleum Engineers, 2012.
[38] J. Romanuka, et al., Low salinity EOR in carbonates, in: SPE Improved Oil Recovery Symposium, Society of Petroleum Engineers, 2012.
[39] Z. Yi, H.K. Sarma, Improving waterflood recovery efficiency in carbonate reservoirs through salinity variations and ionic exchanges: a promising low-cost "smart-waterflood" approach, in: Abu Dhabi International Petroleum Conference and Exhibition, Society of Petroleum Engineers, 2012.
[40] A. Zahid, A.A. Shapiro, A. Skauge, Experimental studies of low salinity water flooding carbonate: a new promising approach, in: SPE EOR Conference at Oil and Gas West Asia, Society of Petroleum Engineers, 2012.
[41] W. Alameri, et al., Wettability alteration during low-salinity waterflooding in carbonate reservoir cores, in: SPE Asia Pacific Oil & Gas Conference and Exhibition, Society of Petroleum Engineers, 2014.
[42] H. Mahani, et al., Insights into the mechanism of wettability alteration by low-salinity flooding (LSF) in carbonates, Energy Fuel. 29 (3) (2015) 1352–1367.
[43] S.J. Fathi, T. Austad, S. Strand, "Smart water" as a wettability modifier in chalk: the effect of salinity and ionic composition, Energy Fuel. 24 (4) (2010) 2514–2519.
[44] N.R. Morrow, J.S. Buckley, Improved oil recovery by low-salinity waterflooding, J. Petrol. Technol. 63 (05) (2013) 106–112.
[45] J.J. Sheng, Critical review of low-salinity waterflooding, J. Petrol. Sci. Eng. 120 (2014) 216–224.
[46] G.J. Hirasaki, Wettability: fundamentals and surface forces, SPE Form. Eval. 6 (02) (1991) 217–226.
[47] J.S. Buckley, K. Takamura, N.R. Morrow, Influence of electrical surface charges on the wetting properties of crude oils, SPE Reservoir Eng. 4 (03) (1989) 332–340.
[48] J.S. Buckley, Y. Liu, Some mechanisms of crude oil/brine/solid interactions, J. Petrol. Sci. Eng. 20 (3) (1998) 155–160.
[49] J.S. Buckley, Y. Liu, S. Monsterleet, Mechanisms of wetting alteration by crude oils, SPE J. 3 (01) (1998) 54–61.
[50] S. Dubey, P. Doe, Base number and wetting properties of crude oils, SPE Reservoir Eng. 8 (03) (1993) 195–200.
[51] J.S. Buckley, et al., Asphaltenes and crude oil wetting: the effect of oil composition, SPE J. 2 (1997) 107–119.
[52] L. Yu, J. Buckley, Evolution of wetting alteration by adsorption from crude oil, SPE Form. Eval. 12 (01) (1997) 5–12.
[53] L. Liu, J.S. Buckley, Alteration of wetting of mica surfaces, J. Petrol. Sci. Eng. 24 (2) (1999) 75–83.
[54] C. Drummond, J.N. Israelachvili, Surface forces and wettability, J. Petrol. Sci. Eng. 33 (1) (2002) 123–133.
[55] W. Anderson, Wettability literature survey-part 2: wettability measurement, J. Petrol. Technol. 38 (11) (1986) 1,246–1,262.
[56] J.N. Israelachvili, Intermolecular and Surface Forces: Revised Third Edition, Academic press, 2011.
[57] A.W. Adamson, A.P. Gast, Physical Chemistry of Surfaces, 1967.
[58] A. Mennella, N.R. Morrow, X. Xie, Application of the dynamic Wilhelmy plate to identification of slippage at a liquid-liquid-solid three-phase line of contact, J. Petrol. Sci. Eng. 13 (3) (1995) 179–192.
[59] R.A. Nasralla, H.A. Nasr-El-Din, Double-layer expansion: is it a primary mechanism of improved oil recovery by low-salinity waterflooding? SPE Reservoir Eval. Eng. 17 (01) (2014) 49–59.
[60] R.A. Nasralla, M.A. Bataweel, H.A. Nasr-El-Din, Investigation of wettability alteration and oil-recovery improvement by low-salinity water in sandstone rock, J. Can. Petrol. Technol. 52 (02) (2013) 144–154.
[61] H. Mahani, et al., Kinetics of low-salinity-flooding effect, SPE J. 20 (1) (2015) 8–20.
[62] E. Hilner, et al., The effect of ionic strength on oil adhesion in sandstone–the search for the low salinity mechanism, Sci. Rep. 5 (2015) 9933.
[63] K.J. Webb, C.J.J. Black, G. Tjetland, A laboratory study investigating methods for improving oil recovery in carbonates, in: International Petroleum Technology Conference, International Petroleum Technology Conference Doha, Qatar, 2005.
[64] D.J. Ligthelm, et al., Novel waterflooding strategy by manipulation of injection brine composition, in: EUROPEC/EAGE Conference and Exhibition, Society of Petroleum Engineers, 2009.
[65] P. McGuire, et al., Low salinity oil recovery: an exciting new EOR opportunity for Alaska's North Slope, in: SPE Western Regional Meeting, Society of Petroleum Engineers, 2005.
[66] T. Austad, A. RezaeiDoust, T. Puntervold, Chemical mechanism of low salinity water flooding in sandstone reservoirs, in: SPE Improved Oil Recovery Symposium, 2010.
[67] M.D. Jackson, D. Al-Mahrouqi, J. Vinogradov, Zeta potential in oil-water-carbonate systems and its impact on oil recovery during controlled salinity water-flooding, Sci. Rep. 6 (2016), 37363.
[68] G. Sposito, The Chemistry of Soils, Oxford university press, 2008.
[69] K. Marinova, et al., Charging of oil-water interfaces due to spontaneous adsorption of hydroxyl ions, Langmuir 12 (8) (1996) 2045–2051.
[70] K.N. Kudin, R. Car, Why are water-hydrophobic interfaces charged? J. Am. Chem. Soc. 130 (12) (2008) 3915–3919.
[71] T. Underwood, et al., Molecular dynamic simulations of montmorillonite–organic interactions under varying salinity: an insight into enhanced oil recovery, J. Phys. Chem. C 119 (13) (2015) 7282–7294.
[72] B. Suijkerbuijk, et al., The development of a workflow to improve predictive capability of low salinity response, in: International Petroleum Technology Conference, 2013.
[73] S. Berg, et al., Direct experimental evidence of wettability modification by low salinity, Petrophysics 51 (5) (2010) 314.
[74] F. Mugele, et al., Ion adsorption-induced wetting transition in oil-water-mineral systems, Sci. Rep. 5 (2015), 10519.
[75] R. Schoch, J. Han, P. Renaud, Transport phenomena in nanofluidics, Rev. Mod. Phys. 80 (3) (2008) 839–883.
[76] E.J.W. Verwey, J.T.G. Overbeek, Theory of the Stability of Lyophobic Colloids, Elsevier, Amsterdam, 1948.
[77] D.C. Grahame, Diffuse double layer theory for electrolytes of unsymmetrical valence types, J. Chem. Phys. 21 (6) (1953) 1054–1060.
[78] R. Hogg, T. Healy, D. Fuerstenau, Mutual coagulation of colloidal dispersions, Trans. Faraday Soc. 62 (1966) 1638–1651.
[79] S.H. Behrens, D.G. Grier, The charge of glass and silica surfaces, J. Chem. Phys. 115 (14) (2001) 6716–6721.
[80] M. Wang, A. Revil, Electrochemical charge of silica surfaces at high ionic strength in narrow channels, J. Colloid Interface Sci. 343 (1) (2010) 381–386.
[81] A. Kitamura, et al., Analysis of adsorption behavior of cations onto quartz surface by electrical double-layer model, J. Nucl. Sci. Technol. 36 (12) (1999) 1167–1175.
[82] J.A. Davis, R.O. James, J.O. Leckie, Surface ionization and complexation at the oxide/water interface: I. Computation of electrical double layer properties in simple electrolytes, J. Colloid Interface Sci. 63 (3) (1978) 480–499.
[83] P. Van Cappellen, et al., A surface complexation model of the carbonate mineral-aqueous solution interface, Geochem. Cosmochim. Acta 57 (15) (1993) 3505–3518.
[84] A. Hiorth, L.M. Cathles, M.V. Madland, The impact of pore water chemistry on carbonate surface charge and oil wettability, Transport Porous Media 85 (1) (2010) 1–21.
[85] H. Mahani, et al., Electrokinetics of carbonate/brine interface in low-salinity waterflooding: effect of brine salinity, composition, rock type, and pH on ζ-potential and a surface-complexation model, SPE J. 22 (01) (2017) 53–68.
[86] P. Moulin, H. Roques, Zeta potential measurement of calcium carbonate, J. Colloid Interface Sci. 261 (1) (2003) 115–126.
[87] A. Pierre, et al., Calcium as potential determining ion in aqueous calcite suspensions, J. Dispersion Sci. Technol. 11 (6) (1990) 611–635.
[88] C.S. Tian, Y.R. Shen, Structure and charging of hydrophobic material/water interfaces studied by phase-sensitive sum-frequency vibrational spectroscopy, Proc. Natl. Acad. Sci. U. S. A. 106 (36) (2009) 15148–15153.
[89] Y.R. Shen, V. Ostroverkhov, Sum-frequency vibrational spectroscopy on water interfaces: polar orientation of water molecules at interfaces, Chem. Rev. 106 (4) (2006) 1140–1154.
[90] K. Roger, B. Cabane, Why are hydrophobic/water interfaces negatively charged? Angew. Chem. 124 (23) (2012) 5723–5726.
[91] D.Y.C. Chan, D.J. Mitchell, The Free-Energy of an electrical double-layer, J. Colloid Interface Sci. 95 (1) (1983) 193–197.
[92] D. McCormack, S.L. Carnie, D.Y. Chan, Calculations of electric double-layer force and interaction free energy between dissimilar surfaces, J. Colloid Interface Sci. 169 (1) (1995) 177–196.
[93] N.R. Morrow (Ed.), Interfacial Phenomena in Petroleum Recovery, CRC Press, 1990.
[94] A. Sharma, Equilibrium contact angles and film thicknesses in the apolar and polar systems: role of intermolecular interactions in coexistence of drops with thin films, Langmuir 9 (12) (1993) 3580–3586.
[95] N.J. Hadia, et al., Laboratory investigation on effects of initial wettabilities on performance of low salinity waterflooding, J. Petrol. Sci. Eng. 105 (2013) 18–25.
[96] S. Das, S. Chakraborty, Steric-effect-induced enhancement of electrical-double-layer overlapping phenomena, Phys. Rev. E - Stat. Nonlinear Soft Matter Phys. 84 (1 Pt 1) (2011), 012501.
[97] E. Gongadze, U. Van Rienen, A. Iglic, Generalized stern models of the electric double layer considering the spatial variation of permittvity and finite size of ions in saturation regime, Cell. Mol. Biol. Lett. 16 (4) (2011) 576–594.
[98] A. Iglič, E. Gongadze, K. Bohinc, Excluded volume effect and orientational ordering near charged surface in solution of ions and Langevin dipoles, Bioelectrochemistry 79 (2) (2010) 223–227.
[99] S. Das, S. Chakraborty, S.K. Mitra, Redefining electrical double layer thickness in narrow confinements: effect of solvent polarization, Phys. Rev. E - Stat. Nonlinear Soft Matter Phys. 85 (5 Pt 1) (2012), 051508.
[100] E. Gongadze, et al., Spatial variation of permittivity of an electrolyte solution in contact with a charged metal surface: a mini review, Comput. Meth. Biomech. Biomed. Eng. 16 (5) (2013) 463–480.
[101] A.G. Volkov, et al., Electrical double layers at the oil/water interface, Prog. Surf. Sci. 53 (1) (1996) 1–134.